Master Thesis | Tesis de Maestría

submitted within the UNIGIS MSc programme

presentada para el Programa UNIGIS MSc

at/en

Interfaculty Department of Geoinformatics- Z_GIS

Departamento de Geomática – Z_GIS

University of Salzburg | Universidad de Salzburg

Plant height and biomass estimations on wheat using high-resolution aerial imagery in an experimental field in Sonora, Mexico

Estimaciones de altura de planta y biomasa en trigo usando imágenes aéreas de alta resolución en un campo experimental en Sonora, México

by/por

Lorena González Pérez
01655587

A thesis submitted in partial fulfilment of the requirements of
the degree of
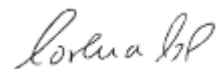Master of Science– MSc

Advisor | Supervisor:

Harald Schernthanner PhD

Ciudad Obregón - Mexico, September 4, 2019

SCIENCE COMMITMENT

Through this document, including my personal signature I certify and guarantee that my thesis is completely the result of my own work. I have cited all the sources that I have used in my thesis and in all cases I have specified their origin.

Ciudad Obregón – Mexico, September 4, 2019

DEDICATED

To me. Because I am worth all this effort and more.

AKNOWLEDGEMENTS

ABSTRACT

At present, one of nine persons living in our world are undernourished. To improve this situation, there are already many global efforts to improve food security, including those that seek to increase crop productivity of small farmers through providing better crop varieties. Wheat is an important source of food intake for many communities, especially in developing countries, and wheat is a key crop for global food security. Thus, the work of physiological improvement of wheat crop is important and can contribute to accelerate genetic gains using new technologies of genomic selection, which take advantage of phenotyping and genotyping of crop varieties.

The present study focused on the contribution to high throughput phenotyping (HTP), which is currently a bottleneck in the process of genomic selection in plant breeding. Estimations of plant height and biomass above ground in wheat crop were obtained using high resolution aerial images from unmanned aerial vehicles in an experimental field in Sonora, Mexico. Two different image resolutions (0.5 cm and two cm), and two different methods of georeferencing of the digital three-dimensional model were evaluated (using ground control points compared to using geotagging of images during image-acquisition and also using a differential correction method of the satellite navigation system).

The study reveals promising results in the estimation of plant height and above-ground biomass. While carrying out the research process, important observations have been made in order to improve the data collection process in future work, especially when repeating the workflows in ongoing breeding programs. The direct georeferencing method using the differential correction has been identified to be the better option, especially, because it is saving time and costs in the data collection process.

Keywords: Plant height, biomass, wheat, photogrammetry, UAV

RESUMEN

Actualmente una de cada nueve personas en el mundo está desnutrida. Ya existen diversos esfuerzos globales para mejorar esta situación, incluyendo los que buscan el incremento de la productividad de los pequeños agricultores por medio de mejores variedades de cultivos. El trigo es una importante fuente de alimento para la humanidad y puede ser clave para la seguridad alimentaria global. Asimismo, los trabajos de mejoramiento fisiológico de trigo pueden contribuir a obtener ganancias genéticas más rápidamente utilizando las nuevas tecnologías de selección genómica que aprovechan la fenotipificación y genotipificación de las variedades.

El presente trabajo se enfocó en una contribución para la fenotipificación de alto rendimiento, que actualmente es el proceso que genera un cuello de botella en el mejoramiento mediante selección genómica en plantas. Se realizaron estimaciones de altura de planta y biomasa encima del suelo en trigo utilizando imágenes aéreas de alta resolución en un campo experimental, utilizando vehículos aéreos no tripulados en Sonora, México. Se evaluaron dos resoluciones diferentes de imágenes (medio centímetro y dos centímetros) y dos métodos para asignar referencia geográfica al modelo tridimensional digital generado (utilizando puntos de control en tierra y haciendo geoetiquetado de las imágenes directamente en el momento de la captura, y utilizando una corrección diferencial del sistema de navegación satelital).

Se encontraron resultados prometedores para estimar la altura de planta y biomasa, como en otros trabajos de la literatura relacionada, pero con correlaciones moderadas. Se detectaron puntos importantes a considerar para mejorar la toma de datos al utilizar estos flujos de trabajo directamente en el mejoramiento. La georreferenciación directa con corrección diferencial se muestra como una opción válida y que puede ahorrar tiempo en la colección de datos.

Palabras clave: altura de planta, biomasa, trigo, fotogrametría, dron

TABLE OF CONTENTS

GLOSSARY

3D	Tridimensional
AGB	Above ground biomass
BM	Biomass
CENEB	*Centro Experimental Norman Ernest Borlaug* (Spanish)
CIMMYT	International Maize and Wheat Improvement Center (Spanish)
CSM	Crop surface model
DEM	Digital elevation model
DGPS	Differential Global Positioning System
DSM	Digital surface model
DTM	Digital terrain model
ERTS	Earth Resources Technology Satellite
GCP	Ground Control Point
GIS	Geographic Information Systems
HI	Harvest index
HSV	Hue, Saturation and Value
HTP	High throughput phenotyping

ICTs	Information and communication technologies
IoT	Internet of Things
LAB	Luminosity, "a" vector and the "b" vector
MVS	Multi-view stereopsis
NASA	National Aeronautics and Space Administration
NDVI	Normalized Difference Vegetation Index
nDSM	Crop surface model
NIR	Near infrared
PH	Plant height
RGB	Red, Green and Blue
RMSE	Root mean square error
RTK	Real-time Kinematics
SDG2	Second Goal of the Sustainable development goals
SFM	Structure from motion
SIFT	Scale-invariant feature transform
UAV	Unmanned Aerial Vehicle

LIST OF FIGURES

LIST OF TABLES

1 INTRODUCTION

1.1 BACKGROUND

From every nine people in the world, one is undernourished (FAO, IFAD, UNICEF, WFP and WHO, 2018). There are many global efforts to alleviate this situation. These efforts are aligned to the United Nations' second goal of the sustainable development goals (SDG2) for 2030: "End hunger, achieve food security and improved nutrition and promote sustainable agriculture" (UN, 2015, p. 15). To fulfill the SDG2, the development of rural areas is essential, as this is where most of the affected people live. Numerous attempts to achieve the SDG2 are focused on improved food systems that drive agro-industrial development, the increase of small-scale farmers' productivity, the support of policy-makers and development programs, among others (FAO, 2017).

Wheat (*Triticum spp*), being the cereal with major production and consumption worldwide (FAO, 2018), is an important source of food for humanity. It is a key crop for achieving food security and to alleviate hunger. However, its production faces environmental and social challenges that mostly affects small-scale farmers in rural areas, *e.g.* unfavorable weather conditions that threaten to lower yield (FAO, 2018).

To improve small-scale farmers' productivity, international crop improvement centers and universities are developing improved varieties, *i.e.* heat, drought, pests or disease resistant high-yielding varieties. As one of the many examples of positive outcomes from crop improvement efforts, the South Asia region has increased its production as much as six times after introducing improved varieties, also known as lines, from the International Center of Maize and Wheat improvement (CIMMYT) (Pask et al., 2014).

Some departments of crop improvement institutions are working on physiological trait-based breeding. In this breeding method, efforts focus on the acquisition of measurements for better understanding the processes during plant growth and development and related biophysical characteristics. For physiological trait-based breeding, extensive in-field manual measurements in experimental plots of hundreds or thousands of entries are requiered, looking at key traits like plant height, days to the growth stages, leaf wax, canopy

temperature, plant biomass, among many others. These traits are important to evaluate because they influence important characteristics such as yield or disease resistance. Measurements of large samples are normally related to high costs in labor and time, and they imply destructive methods on biomass, thus can only be implemented in reduced number of samples.

Since recent years, there are continuous improvements in workflows for data acquisition, processing and delivery of actionable insights by using information and communication technologies (ICTs). Currently, it is possible to have instruments and take measurements from the field continuously using ICTs. Using sensors in a network of internet of things (IoT) enables now important crop measurements like temperature or vegetative indexes to be analyzed and visualized in online maps in real time (Tzounis, Katsoulas, Bartzanas, & Kittas, 2017).

Remote sensing technologies, specially unmanned aerial vehicles (UAVs), have become less expensive in recent years. Thus, they have become more accesible for measurements in agricultural research, making it possible to use them for performing high throughput phenotyping (HTP) of plant traits. Plant height and biomass above ground of wheat and other crops has been succesfully estimated with laser technology (Pittman, Arnall, Interrante, Moffet, & Butler, 2015), true color imagery (Walter, Edward, McDonald, & Kuchel, 2018; De Souza, Camargo Lamparelli, Rocha, & Magalhães, 2017) and combinations of sensors (Geipel, Link, & Claupein, 2014). Nevertheless, these innovative technologies also come with new challenges. They require innovative thinking and new research design approaches to use them to solve modern challenges in agriculture.

The area of interest in the present study, the CIMMYT CENEB station (Centro Experimental Norman Ernest Borlaug from the International Maize and Wheat Improvement Center, in Spanish acronym) in Mexico, consists of 160 Ha of experimental wheat and maize improvement plots, from which different measurements are recorded every crop cycle. However, most measurements are done manually. During the last five years, efforts have been made to modernize the data capture process and analysis. Handheld sensors have been used to measure the Normalized Difference Vegetation Index (NDVI) to assess plant

vigor and greenness, canopy temperature to study heat adaptation, and light interception to assess ground cover percent of the leaves, etcetera. Tablets are used to record plant phenology observations and barcodes to identify samples. Manned and unmanned aerial vehicles are used to transport remote sensors. The technology proficient departments have implemented these new and innovative data capture methods, but there is still no widespread use in all the experiments. To use them in improvement programs these HTP alternatives need to be validated and an efficient workflow should be available first.

The present study focuses on generating a 3D photogrammetry reconstruction of an experimental wheat trial in CIMMYT CENEB station using a UAV (also known as drone). Wheat plot biomass and height were estimated as a low-cost alternative for HTP. Two options for the appropriate image resolution and georeferencing method to create an efficient workflow were evaluated throughout the study.

1.2 OBJECTIVES

1.2.1 GENERAL OBJECTIVE

Estimate wheat biomass on experimental plots through a 3D model-reconstruction using an unmanned aerial vehicle during the winter cycle 2016-2017 in the CENEB experimental station, Sonora, México.

1.2.2 SPECIFIC OBJECTIVES

1. Estimate plant height from photogrammetry data at different resolutions and georeferencing methods.

2. Estimate plant biomass using plot volume from 3D model reconstruction at different resolutions and georeferencing methods.

3. Compare estimated plant height and plant volume from photogrametric evaluation with traditional field manual measurements of these traits.

4. Identify the most suitable resolution and georeferencing method for estimating plant height and biomass from aerial photogrametry.

1.2.3 RESEARCH QUESTION

Different interrogations have inspired the development of these investigation. These are some of them:

- What is the correlation between manually measured plant height compared to estimations obtained from a photogrammetric 3D model-reconstruction of wheat breeding experimental plots at key stages of the crop development?
- What is the correlation between measured biomass compared to estimations of volume obtained from a photogrammetric 3D model-reconstruction of wheat breeding experimental plots at key stages of the crop development?
- What is the optimal image resolution for the 3D model reconstruction of wheat breeding experimental plots for plant height and volume estimations at key stages of the crop development?
- What is the difference in spatial accuracy of real-time kinematics (RTK) correction on the UAV location compared to the use of ground control points (GCP) in the field to georeference the imagery products?

The objectives of this work have been designed to answer as fully as possible the research questions while staying within the limits of the scope of the thesis.

1.3 HYPOTHESIS

The hypothesis is that it is possible to estimate accurately wheat biomass in experimental trials by using the plant height and plot volume through 3D reconstruction made from high resolution images acquired and geotagged with a fixed-wing unmanned aerial vehicle with real time kinematic position correction, without the need of ground control points.

1.4 JUSTIFICATION

The physiological wheat breeding approach has already contributed with significant genetic gains in different countries. It complements the traditional breeding by characterizing the genetic resources available and allows the design of crossing strategies based on known desirable characteristics and to increase the probability to pass them to the next generations of varieties, hence accumulating genetic improvements. The characterization includes the genetic data (genotyping) and the observable characteristics expressed in the field in a specific environment, *i.e.* phenotype (phenotyping) (Reynolds & Langridge, 2016).

By using the combined power of genotyping and phenotyping in physiological breeding, the time needed to produce new varieties can be shortened substantially. Breeding cycles are accelerated through pre-selection of varieties with desirable traits based on "genomic selection" models that are trained with data from characterized varieties. Subsequently, field evaluation is used to predict the most promising lines. With sufficient information, lines don't need to be evaluated in the field before being selected as parents for the next cycle, accelerating the breeding process (Heffner, Sorrells, & Jannink, 2009). The Figure 1 shows a diagram of the genomic selection process, showing how the genotyping and phenotyping of training population can help in the selection process of the genomic selection.
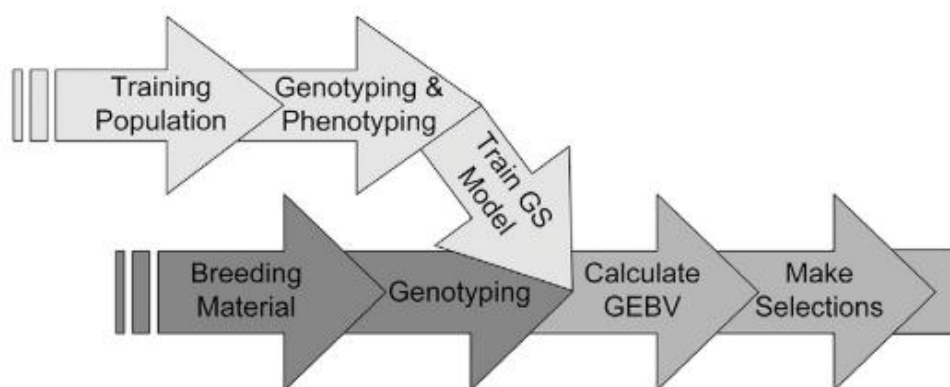
Figure 1. Diagram of the genomic selection process. From Heffner et al., 2009.

Field evaluations involve measuring multiple traits on hundreds or thousands of small wheat parcels. Traditionally they are done manually by human observation or the use of

handheld tools. There are several remarkably interesting crop traits identified for physiological breeding. For the scope of this study, plant height is an important trait to measure for the improvement of grain yield and quality as it is correlated with the harvest index, carbohydrate storage capacity and susceptibility to lodging (Pask, Pietragalla, Mullan, & Reynolds, 2012). Above ground biomass (AGB) is also an important trait related to yield, being related to the harvest index (HI) and radiation use efficiency (Walter et al., 2018).

Making measurements in thousands of plots is time and labor consuming and expensive, adding one drawback in crop improvement. However, technology is in a point where these important measurements can be done faster and accurately, presenting the opportunity to perform HTP to improve the accuracy of genomic selections for grain yield in wheat improvement programs (Rutkoski et al., 2016). Data collection using sensors has been documented to reduce the data collection time by a factor of 60 (Pittman et al., 2015).

In the present study, RGB imagery collected from a UAV is presented because it is a cheaper option regarding the hardware acquisition compared to alternatives like, for example LIDAR or multispectral cameras which have also been used to estimate plant height and biomass (Pittman et al., 2015; Geipel et al., 2014). In the flight mission it may be faster the acquisition, because no radiometric calibrations are mandatory like they are for multispectral cameras capturing reflectance.

Additionally, image georeferencing methods and different resolutions are compared because they are important settings to plan before acquiring remote sensing data. These parameters have an impact in the data quality and ability to represent the characteristics of the observed features as well as in the data processing time. Depending on the selected georeferencing method, different amount of field work will be needed, as well as user interaction in the data processing. Similarly, depending on the image resolution chosen to capture the data, the represented scale of the objects will be different, and the capture time will be typically longer at higher resolutions.

In the case of the study area, in CENEB experimental station, plant height and biomass measurements are being measured manually in several trials where physiological qualities

are studied to complement the breeding process. Substantial investment is made in the labor force needed for these measurements, and a compromise is made to measure subsamples of the full trials or repeating at limited stages because of efforts needed to perform the samplings. Moreover, in these manual measurements are prone to subjectivity and human error. The organization recognizes the need and possibility to adopt the modern technology to increase work efficiency and is open to explore the available options.

1.5 SCOPE

This masters thesis is a correlational study with a quantitaive approach in a wheat experimental field of 0.5 hectares in CENEB station in Sonora, Mexico from the cycle 2016-2017. UAV aerial imagery of two cm and 0.5 cm spatial resolution is used. The spatial accuracy is in the range of three times the image resolution. Tabular results will highlight the correlation differences obtained when using higher or lower image resolution and GCP or direct RTK georeferencing method when estimating plant height and biomass with UAV 3D photogrametric reconstruction on wheat in experimental conditions. The results could be used by wheat breeders in different locations of the globe using very high resolution remote sensors in the visible spectrum to optimize their image acquisition workflows.

2 LITERATURE REVIEW

2.1 PLANT HEIGHT AND BIOMASS IN EXPERIMENTAL TRIALS

As Curtis, Rajaram and Gómez Macpherson (2002) mention, wheat can adapt to a wide variety of environments where it is grown around the world thanks to the complex nature of its genome, even though it naturally thrives in cool environments. Also, they mention it has a development cycle that can go from 120 to 200 days: the duration of each development stage varies depending on genotype, temperature, day-length and sowing date. Important stages of development include booting, anthesis and Maturity.

Monitoring the canopy biophysical parameters helps to understand crop development (Schirrmann et al., 2016). The integration of plant physiology into crop breeding around the green revolution made it possible (Reynolds, Pask, & Muller, 2012). Plant height (PH) and biomass (BM) are relevant traits for cop improvement programs. These type of phenotype traits can be used in genomic selection models to accelerate breeding (Heffner et al., 2009).

Plant height is useful for the assessment of susceptibility of lodging (Berry, Sterling, Baker, Spink, & Sparkes, 2003) or quantification it, to evaluate varieties in water stress models and can be a proxy measure for flowering if monitored continually (Madec et al., 2017). There is a useful correlation between plant height and yield and the plant carbohydrate storage capacity (Pask et al., 2012).

Biomass is an indicator of crop growth. It is an important measure to calculate radiation use efficiency, characterization of wheat morphology and plant organ partitioning as well as nutrients and metabolite analysis. It is a trait of interest in breeding programs. Identifying the genotypes which are able to maintain biomass production during stress conditions implies identifying better adapted lines (Pask et al., 2012). Biomass can be estimated to obtain the HI (Walter et al., 2018), and based on it yield can be calculated (Kemanian, Stöckle, Huggins, & Viega, 2007). The estimation of biomass is essential in relation to nitrogen content measurement, because N is proportional to dry matter (Bareth et al., 2016). The important relationship of biomass with crop development has translated

into multiple efforts towards its assessment (Bendig et al., 2014; Brocks & Bareth, 2018; Pittman et al., 2015).

Despite their importance in crop improvement, measuring plant height and biomass by the traditional method involves plot by plot manual measurements, which is time consuming and labor-intensive activity that does not allow efficient data capture workflows (Guan, Liu, Ma, & Yu, 2018). Also, in the case of biomass measurements it makes impossible the following growth of the crop because it is a destructive approach.

2.2 REMOTE SENSING IN EXPERIMENTAL TRIALS

Measuring phenotypic traits in experimental plots is beneficial for the wheat improvement. However, manual measurement of such traits is inefficient. Using the available technology, measurements can be done faster and accurately, allowing to perform HTP to accelerate wheat improvement programs (Rutkoski et al., 2016). Data collection using sensors and electronic devices can reduce the data collection up to 60 times and by a factor or ten the data processing time (Pittman et al., 2015).

Traits show variability within experimental units, which is hard to represent with few samples taken in the manual measurement approach. Increasing the samples makes the process longer and inefficient, adding that they can have subjective perception bias. However, a sensor, *i.e.* a digital camera, can practically cover completely a wheat plot in one image, showing the variability of the area in a relatively short time (Holman et al., 2016). The key point is to have a sensor that can measure the needed attribute.

Sensors measure physical properties of the crop or can be used to estimate traits from the distance. Sensors can capture a wide range of the electromagnetic spectrum, including the visible light, and calculate the distance to an object. It is possible to measure with cameras the canopy temperature and canopy color using thermal, visible and infrared cameras (Chapman et al., 2014). Also, it is possible to estimate plant height, vigor, plot biomass and tridimensional (3D) shape of its structure using different methods based on these cameras or laser sensors (Walter et al., 2018; Geipel et al., 2014; Bareth et al., 2016).

In-site sensor measurements have been used to acquire the data, making it more objective and efficiently captured. The sensors have been carried by hand or also mounted on terrestrial portable platforms (Crain et al., 2016). Additionally, aerial platforms have also been used to for phenotyping experimental fields (Holman et al., 2016). The size of the area of interest, the objectives of the work and available resources are factors that determine which sensor and platform is used.

2.2.1 EVOLUTION OF REMOTE SENSING IN AGRICULTURE

Photography set the bases for remote sensing in the visible spectrum of light. During World War II, other sensors were developed for the rest of the electromagnetic spectrum: radar, sonar, and thermal infrared detection systems (Moore, 1979). Platforms have also evolved along with the sensors.

The first satellite imagery mission was the CORONA project. It started successfully in 1960 by the US, urged by the cold war. However, it was classified and used for military purposes only (Ruffner, 1995). The first satellite mission designed to monitor and study earth's surface was launched in 1972 by the United States of America: initially named ERTS (Earth Resources Technology Satellite) and then Landsat 1, which was envisioned to improve the knowledge of the natural resources on earth and help people manage them better, providing quality imagery from the globe (NASA, n.d.).

Since then, remote sensing has been widely used in agriculture. Yield estimates using light use efficiency have been done successfully with satellite multispectral imagery at a regional level (Lobell, Asner, Ortiz-Monasterio, & Benning, 2003) and nitrogen management of crops at field level (Bu, Sharma, Denton, & Franzen, 2017). However, for experimental crop improvement fields, the resolution of satellite imagery is insufficient to identify individual plots.

Marshall, Barnhart, Hottman, Shappee & Most (2012) declare that sensors on UAVs allow fine detail in the size of the smaller observable object (spatial resolution), frequent and flexible data acquisition, ease of use and the adaptation to different mission landscapes

compared to previously available platforms. The UAV as we know it today, started with the first autonomous torpedo successfully launched in 1918. UAVs where restricted to military until 1990. Finally, they also stated that after they proved their value during middle east reconnaissance missions, non-military saw the potential on them to lower their costs in activities they were already doing with manned planes or that where only possible with smaller planes (Marshall et al., 2012).

 As they became more widely used, sensors and aerial platforms have lowered their prices to make them more accessible. They offer the possibility to implement solutions in a wide range of applications for precision agriculture, that involves data-driven actions for optimized agronomic management. Nevertheless, the specific situation should always be considered to choose the most appropriate tools for each study (Shi et al., 2016).

In their study, Shi et al. (2016) have proven the technology useful for the research, but operational workflows are still developing to be able to connect all the people and steps involved in the process: from sensors and technicians collecting the data to the scientists and decision makers. They reported that for all missions, particularly large ones, great planning, coordination and quality control are needed for success. It also was mentioned that with streamlined and organized data collection, decision support tools can be implemented and widely adopted for crop improvement.

According to Tzounis et al. (2017), information technology advancements go along with the sensors and platforms in the modernization and intensification of agriculture: remote sensors can generate massive amounts of data continuously at a fast rate and in different formats. They mention that all that data can be efficiently processed, consolidated from multiple sources and made useful through automated artificial intelligence algorithms to extract actionable information about the observed phenomena, which cannot be measured directly. The term they used for such analysis is "Big data" and to withstand the corresponding workload, the "cloud" technology is used, which means having distributed abundant computational and storage capacity using the internet and multiple hardware stations connected (Tzounis et al., 2017).

Furthermore, Tzounis et al. (2017) affirm the "Internet of things" (IoT) in agriculture is expected to optimize production: it can provide the optimal growing conditions for crops, guide in the most efficient way the resource usage and also adjust production in accordance to the market situation, maximizing the profit and minimizing the costs. Agricultural IoT involves interconnected wireless sensors, machinery, weather stations, internet gateways, computational power, electronic object identifiers, smartphones that generate big data. Finally, they also mentioned the integration with Geographic Information Systems (GIS) for mapping the collected data is essential.

2.2.2 COLOR

According to Poynton (2006), color is the perception of (visible) light by the retina: the eye perceives color through three types of specialized cells called "cones", which are sensitive to slightly different portions of the light spectrum between 400 and 700 nm. He explains that to represent a color, three numeric components are enough if the color-coding system being used is specified too. Various color-coding systems exist, each of them defines the 3 "axes" that allow to identify a specific color in their scale.

Examples of the systems are RGB, HSV and LAB: RGB stands for red, green, blue; HSV stands for hue, saturation, value; LAB represents luminosity, the "a" vector (indicating red or greenness) and the "b" vector (indicating yellow or blueness). In Figure 2, the RGB model is represented as a 3D cube, illustrating how the combinations of the red, green and blue components can generate any of the desired colors. Tuples of values from 0 to 255 for the three variables indicate the color, for examples [255,0,0] in the RGB space denote the red color (seen in the lower left corner) and [255,255,255] represents the white (in the center corner of the figure). In the Figure 3 the HSV system represented as a 3D cylinder is presented and likewise the RGB model, the tuples of values in its own scale will represent the color: [0,100,100] for red (top left of the cylinder) and [0,0,100] for white (center top of the cylinder).
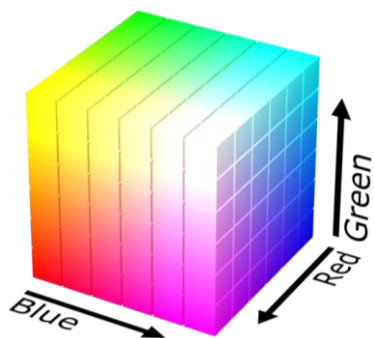
Figure 2. RGB color-coding system represented as cube. From SharkD, 2010b.
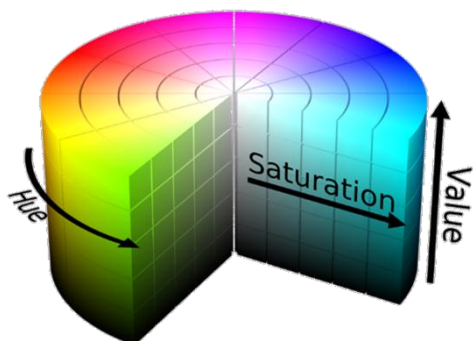
Figure 3. HSV color-system represented as a cylinder. From SharkD, 2010a.

2.2.3 SENSORS

Sensors detect the light from a defined range of the electromagnetic spectrum. The regular digital camera can capture in a two-dimensional matrix of values the incident light in the RGB portions of the electromagnetic spectrum. These delimited parts of the spectrum are called "spectral bands" (Shi et al., 2016). In Figure 4, the RGB bands can be seen in their corresponding colors between the 0.4 µm and 0.7 µm wavelength. The near infrared (NIR) band is from 0.7 µm to approximately one µm. From three to 14 µm the band is called thermal infrared (Albertz, 2007 as cited by Science Education through Earth Observation for High Schools, n.d.).
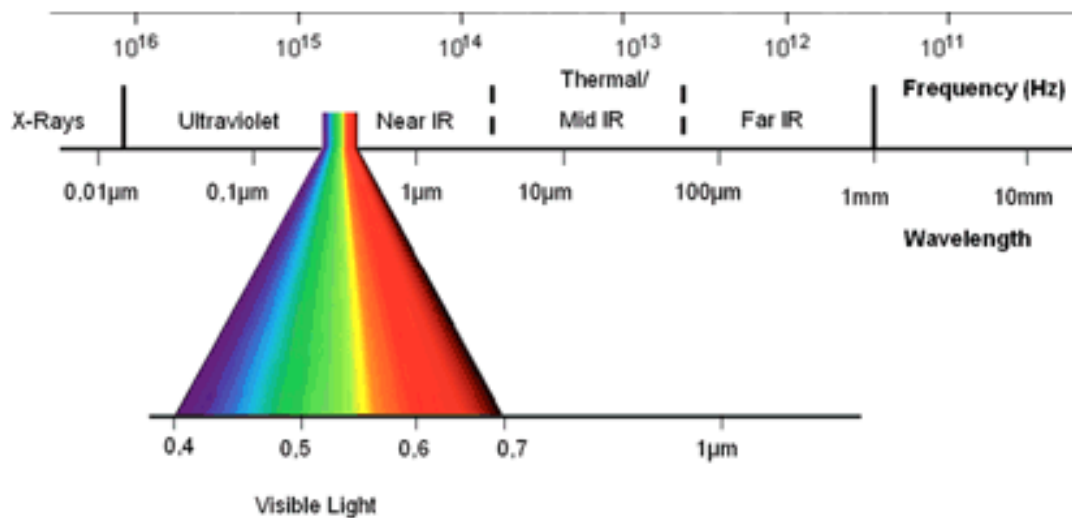
Figure 4. Spectral bands in the visible and infrared. From Albertz, 2007 as cited in Science Education through Earth Observation for High Schools, n.d.

The importance of detecting the light that is reflected from the objects is that their composition will affect how the light is reflected. In the case of remote sensing in agriculture, the electromagnetic radiation interacts with the plant canopy causing some light to be absorbed by the plant, reflected or transmitted through it (Hurcom, Harrison, & Taberner, 1996). Depending on the plant species, variety, growth stage, structure and health the light that a sensor can detect from them will be different. Remote sensing benefits from those properties to identify objects from the distance.

NIR is important in remote sensing vegetation monitoring because the internal cellular structure of the leaves directly influences the reflectance and can be used to assess indirectly the biophysical properties of the plants (Hurcom et al., 1996). Compared to RGB cameras, NIR cameras capture a portion of the light spectrum that human eye cannot see. The significant difference between the red and NIR parts of the spectrum are used to highlight the crop characteristics in band combinations called "vegetation indexes". Figure 5 displays a vegetation spectral profile, showing the percentage of light reflected from a plant in different wavelengths of the visible and NIR light, as well as indications of which cellular structure is influencing the light reflectance at specific points. In the visible part of the spectrum the differences in reflectance are related to the differences in chlorophyll absorption by the leaves.
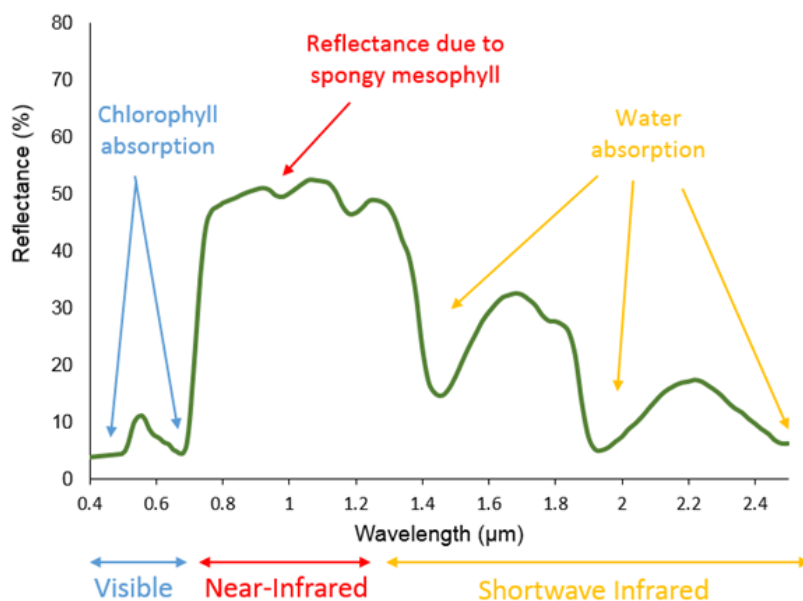
Figure 5. Vegetation spectral reflectance profile. From Humboldt State University, n.d.

The thermal part of the electromagnetic spectrum can be interpreted by the adequate sensors as the temperature of the object, which can be useful in crop monitoring related to water stress (Chapman et al., 2014). Figure 4 shows that thermal bands are typically wider than visible and NIR bands. The band width is related to the need for the sensors to detect the range in the electromagnetic spectrum that contains significant changes that can be used to differentiate the observed surfaces. A camera that can detect more than two ranges separately (bands) is called multispectral. If it can detect dozens of very narrow bands it is called hyperspectral.

Another type of remote sensors are proximity sensors. These can be based on light (Light Detection and Ranging, LIDAR) or ultrasound. These sensors can measure the distance to the observed objects based on wave pulses emitted towards them, reflected back and detected, then based on the distance and the relative position, multiple points representing the visible surface of the object are stored (Tilly, Schiedung, Hoffmeister, & Hütt, 2014). Thus, the 3D shape of the object can be reconstructed digitally (Cheng, Jianya, Li, & Liu, 2011). When a proximity sensor is activated along the canopy of the crop, a 3D cloud point model of the canopy can be generated. Figure 6 shows an example of a LIDAR sensor scanning the objects around it. The laser beam is moving and in the third frame it

can be seen the points that represent where the laser bounced back to the sensor to be detected, forming a digital representation of the objects.
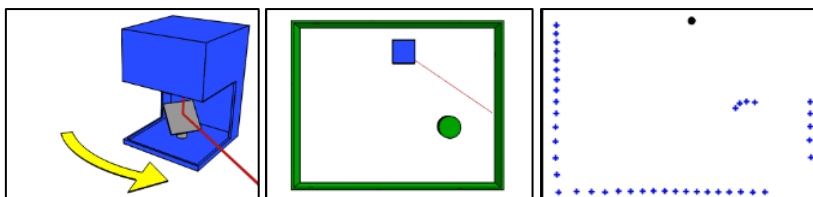
Figure 6. Example of the operation of a scan line of a LIDAR system: 3D, top and result view. From Mike1024, 2008.

2.2.4 PLATFORMS

Sensors are mounted on a wide range of platforms, according to the needs of the project. They can be terrestrial low-cost, low-price platforms able to capture very high level of detail (Crain et al., 2016), fixed locations for intensive and continuous data collection (Brocks & Bareth, 2018), flexible and fast aerial platforms like UAVs (Chapman et al., 2014) or satellites capable of global coverage (Bu et al., 2017). The present work focuses on UAVs.

Different types of UAVs offer different advantages and limitations (Shi et al., 2016). There are two main categories of UAVs: rotary wing and fixed wing, which can be illustrated by comparison to the helicopter and the plane, respectively. Rotary wing UAVs generate lift by displacing air with the rotation of their propellers. Fixed wing UAVs generate lift by the forward airspeed and the aerodynamic profile of the airframe, the propellers generate the forward movement. Rotary wing UAVs can hover still and low over the crop, allowing to get more detailed data. Fixed wing UAVs have longer endurance than the rotary wing UAVs because the lift is produced by the wings and not entirely by the motor; however, they need to always fly faster than its stall speed needed to generate the lift. In general, rotary wing UAVs are more suitable to monitor smaller areas at a greater detail and the fixed wing UAVs can cover larger areas in less time, but at lower level of detail.

2.3 3D CROP RECONSTRUCTION

UAV surveys with different sensors have been used in crops like corn, barley, rice, sugarcane, vine and wheat, among others to measure different traits of direct interest successfully or in some other cases, proxy measurements are acquired to estimate a trait (Bendig, Bolten, & Bareth, 2013; De Souza et al., 2017; Walter et al., 2018; De Castro et al., 2018). Another advantage of the UAVs is that, in contrast to manual measurements where access to the field is necessary, measurements can be done independently to field accessibility constraints. Due to the high resolution achieved by UAVs, observable traits are not only spectral on the field or plot level, but also the shape and structure of a single plant can be identified (Shi et al., 2016). 3D photogrammetric reconstruction is increasingly showing its potential for multi-temporal cost-effective measuring systems (Brocks & Bareth, 2018).

A digital surface model (DSM) is a raster that represents the 3D reconstruction of the elevation of the surveyed visible surface of the earth, including any object on it (Holman et al., 2016). A digital terrain model (DTM) is a raster that represents the 3D surface of the bare soil of a given area, not considering any object present on it (Geipel et al., 2014). A crop surface model (CSM) is a raster that represents the 3D reconstructions of the height of the objects above ground (Bendig et al., 2014). The CSM is the result of subtracting the DTM from the DSM of a given place. Figure 7 shows the mentioned differences, using the label "nDSM" to indicate the CSM, which in this case represents the plant height.
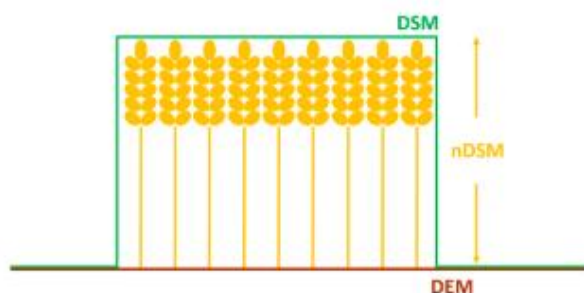
Figure 7. Representation of a DSM, CSM (nDSM) and a DTM (DEM). From Holman et al., 2016.

There are two main approaches for 3D crop reconstruction: photogrammetry and proximity sensors, *i.e.* LIDAR (Shi et al., 2016). Photogrammetry approach was used for the 3D reconstruction focused on crop plots in the current work. It will be presented with more detail below.

2.3.1 PHOTOGRAMMETRY

Photogrammetry is the technique that allows accurate measurements from imagery, currently using digital means (Aber, Marzolff, & Ries, 2010). It is based on the stereoscopic vision to perceive depth, like the mechanism of a pair of eyes that allow to perceive the 3D nature of objects in the environment (Devi, 2014). To obtain the data to represent an area of interest, overlapping images are acquired from different points at the same distance from the terrain, providing multiple points of view for every point observed. Afterwards, the imagery is processed to generate a digital model. Figure 8 shows an example of the imagery collection needed for the photogrammetry process. The red rays represent the extent of the area captured by each aerial image, displaying the overlap needed for the photogrammetric reconstruction of one point viewed from multiple perspectives.
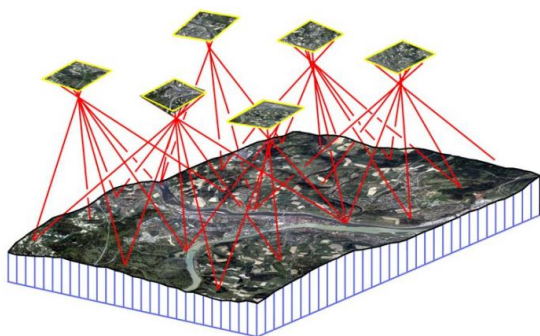
Figure 8. Example of imagery acquired for photogrammetry. From TheHighTechHobbyist, 2016.

Structure from motion (SFM) photogrammetry is a method of 3D reconstruction based on images that capture the same object from different points of view: SFM method can calculate the position of the camera at the time of image capture, its orientation and geometry, providing a digital reconstruction of the (relative) camera locations at the time of image acquisition and the 3D shape of the observed scene (Holman et al., 2016). Multi-view stereopsis (MVS) techniques join photogrammetry and computer vision to generate dense clouds of 3D points representing the observed surface, based on known position and parameters of the cameras that captured the imagery (Harwin & Lucieer, 2012). They use algorithms like scale-invariant feature transform (SIFT) (Lowe, 2004) to find identifiable points present in the overlapping imagery and be able to recreate 3D point model.

The resulting accuracy of SFM algorithms in photogrammetry is limited by factors like image overlap, texture of the surface, the resolution of the imagery, illumination changes, acquisition geometries, platform trajectory, disturbances by strong wind during collection and the irregularity of the terrain (Bendig et al., 2013; Harwin & Lucieer, 2012; De Souza et al., 2017).

During the SFM process, the perspective and lens distortions inherent to the camera imagery can be corrected because the position and orientation of the camera (external orientation), focal length and radial distortion parameters for each photograph (internal orientation) are calculated (Harwin & Lucieer, 2012). When the 3D scene has been reconstructed with point locations along the observed surface, the original pictures are projected and merged (mosaicked) into the digital surface model (DSM) that has been

generated to produce an image free of distortions with uniform scale called orthomosaic. Marshall et al. (2012) explain that the orthomosaic presents an image of the recreated scene as if it had been captured exactly from the top view at every point in it. Imagery georectification process allows to use the image captured with the UAV in GIS and mapping, so they can be stacked over other layers of data based on the known geographic position of the features.

A model quality increases when more photos are used, *i.e.* the features are captured from more diverse perspectives (Walter et al., 2018). However, collecting more photographs also increases collection time, and consequently costs (Bendig et al., 2013). Using a crossed flightpath covering the whole area in perpendicular directions improves the 3D reconstruction. Crossed flightpaths increase the number of images taken from the same area, improves the distribution of the imagery, balances the different brightness captured from different angles and helps to reconstruct better the 3D nature of the objects (De Souza et al., 2017).

UAV platforms using photogrammetry are currently the most widely used approach for crop monitoring because of low cost, high versatility and recent advances in platforms and sensors (Bendig et al., 2013). Currently there is available a variety of commercial and noncommercial photogrammetry software for processing aerial imagery, *e.g.* Pix4Dmapper by the company Pix4D, Metashape by Agisoft, Drone2Map by the Environmental Systems Research Institute, MicMac by the French National Geographic Institute & the French National School for Geographic Sciences and OneButton by Harris Geospatial Solutions.

2.3.2 PHOTOGRAMMETRY VS LIDAR

DEMs generated from imagery do not represent the complex detailed volumes compared to LIDAR point clouds because they are 2.5D structures. Crop canopies represented by a 2.5D surface shows only the most external surface, being unable to represent vertical layers in one point (Monserrat & Crosetto, 2008). LIDAR, in contrast, can penetrate on layers and generate true 3D point clouds because it is not restrained to be a continuous surface.

(Madec et al., 2017). Both methods of 3D reconstruction can produce highly detailed point clouds, although the point density is considerably lower for the UAV-based approach. (Bendig et al., 2014).

LIDAR terrestrial survey appears limited when the system needs to be moved through all the plots in phenotyping platforms, being a time consuming survey (Bareth et al., 2016). However, it can provide at the same time the DSM of the canopy and the DTM. LIDAR survey can be more accurate than manual measurements (Madec et al., 2017). Additionally, it is expensive in comparison to UAV photogrammetry and more specialized skills for the data collection and customized processing workflows are needed (Deery, Jimenez-Berni , Jones , Sirault, & Furbank, 2014)

 The nature of SFM and MVS techniques require multiple points of view for a successful reconstruction (Harwin & Lucieer, 2012). They do not penetrate on the canopy as much as LIDAR due to the occlusions observed when a point is seen from different directions and also because of the spatial resolution (Walter et al., 2018). DTM from crop fields can only be generated directly from photogrammetry if the ground is clearly visible, *e.g.* phenotyping platforms where small plots are divided by bare ground spaces (Holman et al., 2016) or fields with identifiable bare soil spaces between plants. Alternative ways to create the DTM must be considered, for example, making a previous reconstruction of the field when no crop is grown yet.

2.3.3 LOCATION ACCURACY AND SPATIAL RESOLUTION

According to Shi et al. (2016), in the 3D photogrammetry reconstruction, spatial resolution, level of detail, noise, time for acquisition and processing are factors that need to be considered when planning a data collection flight campaign. In their work they make reflect that scientists in the field are developing the best practices for 3D reconstructions of crops. The level of detail influences what scale of a phenomena can be seen (Madec et al., 2017), so the resolution at which a phenomenon is photographed is crucial. Cases of low correlations to ground truth measurements and low genetic variance for UAV data, have

been attributed to coarse resolution issues, however, too high resolution imagery is easier influenced by wind introducing noise to the model, especially when fewer images are available (Madec et al., 2017; Walter et al., 2018).

Accurate georeference is needed when working with experimental plots, because the plots are small and close together. Global Navigation Satellite System (GNSS) receivers, *e.g.* from GPS, allow to know the location of a point, allowing modern commercial UAVs to tag the captured imagery with the location of their acquisition (Geipel et al., 2014). The location metadata on each image is called geotag (Shi et al., 2016). However, the accuracy of these moving measurements is limited to several meters (De Souza et al., 2017). To improve the precision, Differential Global Positioning Systems (DGPS) can be implemented, using a stationary receiver on a previously known position (base) to calculate the instant offset from its true position (Madec et al., 2017). The offset calculations can later be used by the mobile receiver, *i.e.* the UAV, to enhance its calculated position. When the DGPS correction is performed during the survey, *e.g.* transmitted by radio, the technique is called Real Time Kinematic (RTK). Studies using UAV RTK have recently been increasing, given that commercial platforms are recently available (Bendig et al., 2014). Figure 9 shows a diagram of how the DGPS correction works to improve the accuracy of the geographic position of a UAV, using the base receiver to calculate the corrections of the position and sending them to the UAV.

X_{23} y_{23} z_{23}

x_{19} y_{19} z_{19}

x_{14} y_{14} z_{14}

x_{21} y_{21} z_{21}

Measured: X Y Z

Delta: x y z

True: X Y Z

Corrections applied after survey

Known: x y z

Measured: x y z

Delta: x y z
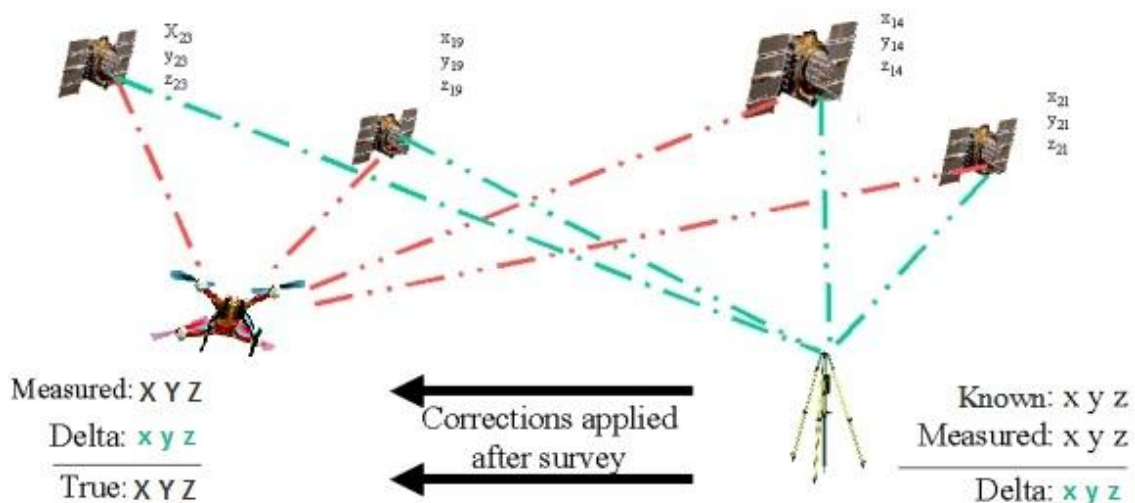
Figure 9. Illustration of the DGPS correction of a moving receiver by a base station. Adapted from NOAA, n.d.

Georectification conventional techniques require visible GCPs in the image, with known accurate location to give the mosaic its true location on earth (Marshall et al., 2012). Highly visible targets need to be distributed in the field to be able to identify and use them as GCPs. A higher number of GCPs and a better distribution increases accuracy (Harwin & Lucieer, 2012; Sanz-Ablanedo, Chandler, Rodríguez-Pérez, & Ordóñez, 2018). Alternatively, the model can be georeferenced directly during the photogrammetric process if the imagery is geotagged. If RTK was used during the flight to get accurate camera location, the SFM algorithm is improved, as well as the georeferenced output orthomosaic. If direct georeferencing is used, replacing the GCPs use, time and costs are saved during data capture (Madec et al., 2017).

A way of evaluating the georeference accuracy of a 3D model is comparing the coordinates calculated in the photogrammetric process, present in the resulting orthomosaic, with the "true" measured coordinates of GCPs. However, a more objective evaluation of the true accuracy can be performed if independent checkpoints, different than the GCP used to georeference the model, are used for the comparison (Sanz-Ablanedo et al., 2018).

There are promising experiments that have explored the possibility to fully georeference the photogrammetric models with the UAV navigation system aided by an RTK correction, without GCP reference (Dall'Asta et al., 2017). This workflow allows to lower the field costs

and data acquisition time, as well as allowing more frequent revisit times in one site or the monitoring of more area. The research evaluating the accuracy of direct georeferencing compared to the use of GCP is still in progress. (Sanz-Ablanedo et al., 2018).

2.4 ESTIMATING WHEAT PLANT HEIGHT

Current plant height measuring methods include measuring manually with a ruler, which is time consuming, low throughput and susceptible to subjective bias or mistakes (Madec et al., 2017), and allows to sample very few of the variability of the crop. LIDAR estimation of plant height using terrestrial platforms shows good results, with R^2=0.86 and RMSE=78.93 mm (Deery et al., 2014; Bendig et al., 2014). Correlation is high between LASER and UAV-derived plant height (R^2 = 0.91) (Bareth et al., 2016).

Accurate plant height estimations using UAV imagery is possible (Walter et al., 2018). Best results are obtained when the values for all the stages are considered for the correlations. Values of the estimations tend to scatter at the later stages, partially due to strong winds during capture, changes in the canopy properties that obstruct MVS reconstruction and lodging when it is present. Comparison of the CSMs for different phenological stages allows the detection of crop growth variability and flowering time estimations (Bendig et al., 2013; Madec et al., 2017; Bareth et al., 2016). Measuring frequently with cameras on fixed poles has been proposed for continuous monitoring, *i.e.* 95 to 129 times per cycle (Brocks & Bareth, 2018). Plant height measurements correlate highly to above ground biomass if the whole cycle is taken into account but are not as descriptive if only one measurement at one stage is observed (R^2 < 0.5) (Madec et al., 2017).

It has been observed that the DSM generated by UAV imagery underestimates height (Bendig et al., 2014; De Souza et al., 2017). Madec et al. (2017) explains this referring to image resolution matching the canopy features at one centimeter and Brocks, Bendig, & Bareth (2016) mention the possibility that wind bends the canopy at the capture time and generates lower measurements. It has been highlighted the significant importance of algorithm used to calculate the plant height from the point cloud or CSM, which will have

a major impact on the results (Walter et al., 2018; Bendig et al., 2014). Different extraction methods have included using the 99.5% percentile, the mean and the mean of the four highest points of the canopy in the crop (Madec et al., 2017; De Souza et al., 2017; Walter et al., 2018). Extracting plant height from the 3D model of the crop, more comprehensive sampling is made and it is more representative than manual measurements (Bareth et al., 2016).

2.5 ESTIMATING WHEAT BIOMASS

There are numerous studies set to measure biomass nondestructively since around 1980s (Brocks & Bareth, 2018), mostly through canopy height and vegetation indexes, but limited number of them accounting for the 3D nature of wheat (Bendig et al., 2014; Geipel et al., 2014; Schirrmann et al., 2016). 3D cloud points have been explored to measure different wheat organs or plant height, but few studies have focused in estimating above ground biomass (Walter et al., 2018).

Linear correlations between plant height and biomass have been observed for the first half of the growing cycle and an exponential function appears to model better the increase of biomass with very small changes in plant height in the second half (Tilly et al., 2014).

Madec et al. (2017) suggested additional variables like plant area to calculate better the volume of the crop, *e.g.* using a greenness index to mask the area covered by the plant using RGB imagery (Wenzhu, Wang, Zhao, Zhang, & Feng, 2015).

In Walter et al. (2018), their approach permitted to photograph each plot and see all the sides, but that is hard to achieve in real phenotyping plots when the canopy closes, and harder to obtain that high image overlap with UAV on a big trial. Linear relationship between 3D point cloud volume and biomass was found with a R^2 =0.79, in a single cultivar with varying seed density treatments in the maturity stage.

3 METODOLOGY

3.1 AREA OF STUDY

This study was carried out in the Yaqui Valley, Sonora, Mexico, at the experimental station from the International Maize and Wheat Improvement Center (CIMMYT). The trial is located at 27.3955 north latitude and 109.9283 west longitude, in the municipality of Cajeme. The Yaqui Valley is located in the north west of Mexico and characterized by intensive irrigated agriculture. Its seashore to the west is open to the Gulf of California.

The Yaqui Valley croplands are of outstanding importance for the agricultural production in Mexico and for the world's wheat improvement. It shares its agroclimate with 40 percent of the land where wheat is grown in the developing countries. It has a semiarid climate with an annual average rainfall rate of 317 mm (Matson, Luers, Seto, Naylor, & Ortiz-Monasterio, 2005).
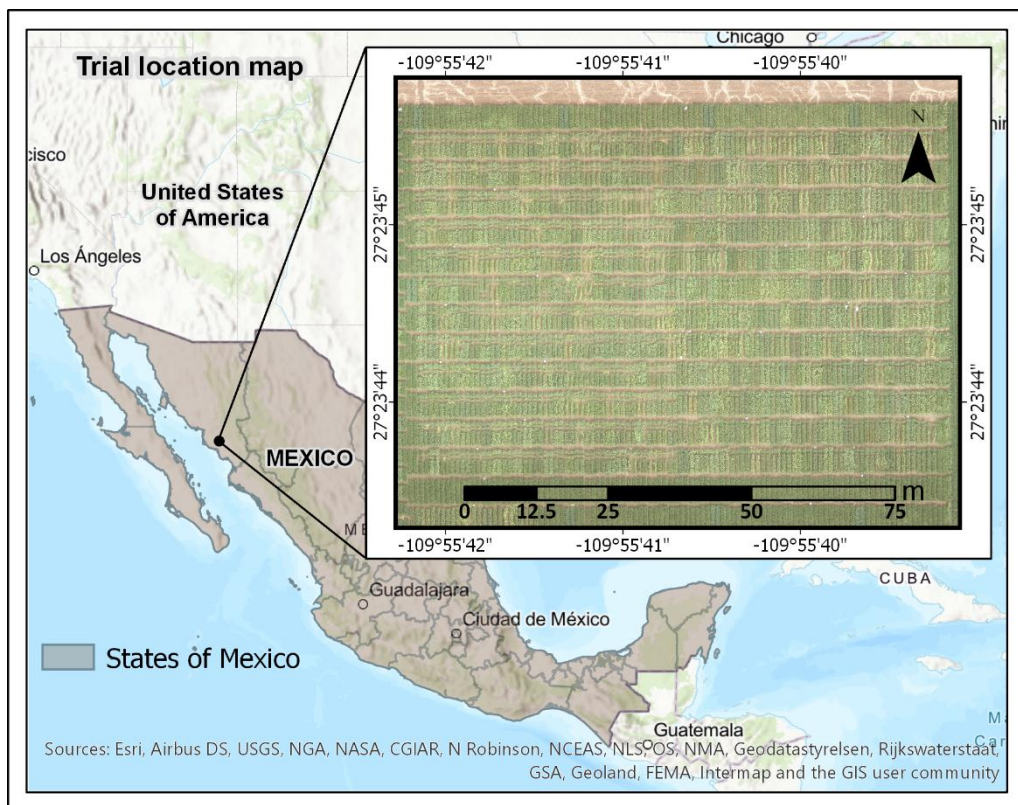
Figure 10. Location map of the study area. UAV image from March 8th, 2017.

3.2 DATA USED FOR THE STUDY

The data acquisition corresponds to a wheat yield trial with 150 genotypes with four randomized replicates in a wheat physiology program during 2016-2017 winter cycle. The plot size is four meters long and two adjacent beds of 0.8 m width each.

All varieties were mechanically planted and harvested at the same time, in november 2016 and april 2017, respectively. At the moment of harvest, the plot size was measured to have an accurate harvest area to compute yield, in case that there was any plot length issue during the cycle. However, due to the genetic differences, sometimes the cultivars reached the growth stages in different days. To be able to make the desired height and biomass measurements at the specific growth stages for every variety, the trial was monitored three times per week to be aware of the appropriate day for the samplings. A map of extent and location of the experiment can be seen in Figure 10. To the left of the RGB image, the marks of the biomass sampling cuts are visible to the north of each plot.

3.3 METHODOLOGICAL STEPS OF THE RESEARCH

A 3D photogrammetric model was used to obtain the estimations of plant height and plot biomass for the current study due to the accessibility of the technology and affordability (Brocks & Bareth, 2018; Bendig et al., 2013), fast data capture (Holman et al., 2016) and the existent evidence of its capability to model crop characteristics of interest (Bendig et al., 2013; De Souza et al., 2017; Walter et al., 2018; De Castro et al., 2018). The plant height was estimated based on the difference of the top of the canopy minus the ground elevation (Brocks & Bareth, 2018; Geipel et al., 2014; Bendig et al., 2014). The volume estimation to compare with the plot biomass was obtained considering the plant height and the green area inside the plot extent (Madec et al., 2017; Walter et al., 2018). The reference measurements of plant height were measured manually with ruler and plot biomass was cut and weighted, as it is the current way to do it in CIMMYT. Finally, Pearson correlation was computed (Chapman et al., 2014) to compare the relationship between the ground measurements of PH and AGB and the aerial estimations of PH and volume, respectively.

The Figure 11 shows a diagram of the processing steps followed to collect, process and analyze the data. In the following sections the steps are explained in detail.
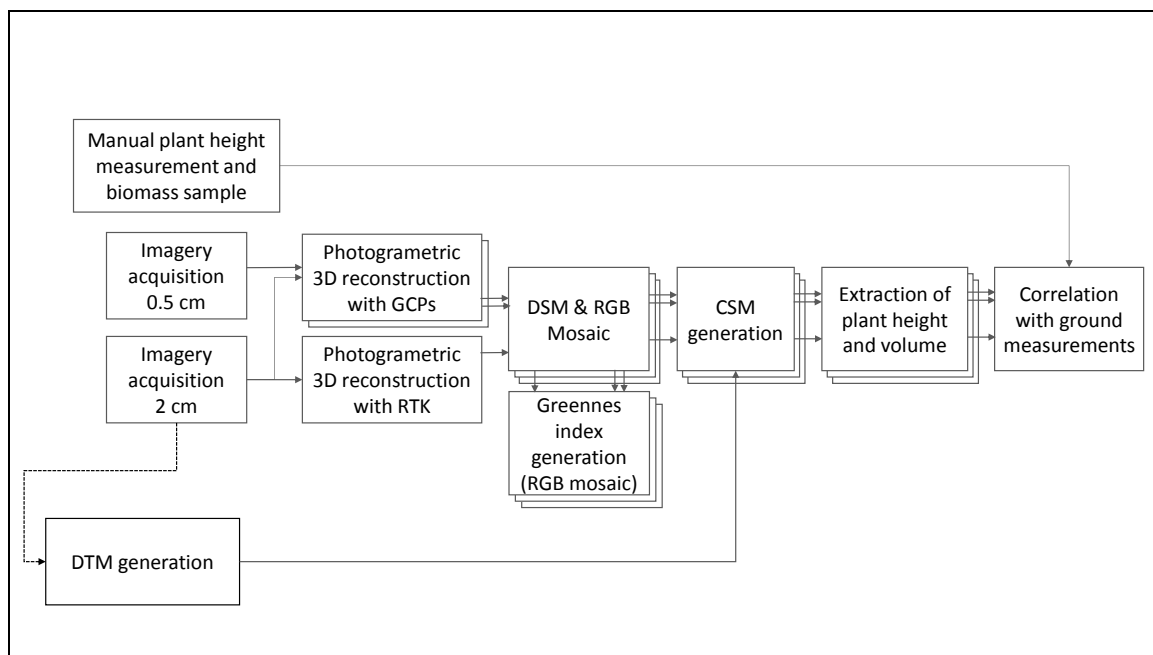
Figure 11. Methodology workflow

3.3.1 MANUAL PLANT HEIGHT MEASUREMENT AND BIOMASS SAMPLING

The plant height and biomass are the two field variables to be compared in this study, trying to estimate from the aerial 3D model. The reference plant height was measured manually for two growth stages during the crop cycle: at the start of booting and seven days after flowering, which are stages of interest for the breeding at CIMMYT. The biomass measurements were collected for 149 varieties and the plant height data for 49 of the varieties in the replicates one and two, due to time and labour limitations. Unfortunately, the data for the plant height at booting stage was lost and no measurements were available for that stage. To recover some data, an extra measurementa was performed on the eighth of March in 96 of the plots where plant height was measured.

The average plant height was measured in each plot in four plants, two in each bed. The data was recorded on paper and then digitized in a spreadsheet. Plants were measured

similarly as it is commonly performed at CIMMYT's physiology department, but with an important difference. For typical yield trials, the height is measured from the soil to the upper part of the spike along the plant shoot, manually holding straight the plant if it was not vertical. For this experiment, height was determined vertically from the ground to the height of the upper part of the spike without accounting for the beards and without moving the plant, even if it was slightly bent. This was decided considering that the measured height would be compared to the one computed from a 3D model where the plants would be captured in their neutral posistion and the height would be computed vertically from the soil surface.

Biomass samples were collected manually at the beginning of boothing stage, seven days after anthesis and after plant maturity. Biomass samples and plant height measurements corresponding to any given plot were performed in the same date for the corresponding stage. The cut area was 50 cm by two beds in the north of each plot, allowing a cut free area of two meters long to the opposite side of the plot for the image data extraction.

The plants collected in the field were put in plastic bags identified with the plot name and weighted in the office to get the fresh biomass. Afterwards, to know the moisture content, a subset sample consisting of 100 shoots (SS100) was weighted again in fresh and then dried in the oven for 24 hours at 98º C to weight again to have the dry biomass and be able to calculate the moisture content percent. The reported biomass is the dry biomass, *i.e.* the weight of the plot plant sample at 0% moisture. The corresponding formula is the next: Biomass = (fresh plant weight) × (dry weight of subsample / fresh weight of subsample) (Pask et al., 2012).

3.3.2 IMAGERY ACQUISITION

The variables involved in this section are the image resolution (two cm and 0.5 cm per pixel) and the accurate georeferencing method (using GCP or the RTK correction on the image location). These variables are needed in the activities to complete the fourth specific objective.

3.3.2.1 PLATFORMS AND SENSORS

The flight campaign was performed along the cycle to match the plant heigth and biomass sampling dates. Two different type of platforms were used to acquire the desired resolution for testing: a fixed-wing and a multirotor UAV. 13 flights were performed with both UAV and one was just performed with the fixed wing.

The fixed-wing, eBee RTK by Sensefly, was used to acquire imagery with a resolution of two centimeter per pixel with an RGB Canon PowerShot 110 camera of 16.2 MegaPixels. The software for the flight planning and geotagging was eMotion by Sensefly company. The eBee has a minimum flight speed of ten m/s, which allows to cover large areas in a single flight, but at the same time it is a limitation if a high image overlap is needed at a very high spatial resolution, *i.e.* at low altitudes, and a limited image capture rate. To be able to improve the overlap, and to get more images, the flight plan was designed with perpendicular flight lines as (De Souza et al., 2017). The flightplan was set to achieve a lateral overlap of 80% and an approximate longitudinal overlapp of 50% in every set of paralel flightlines. Previous studies have used a wide range of image overlap going from 25% to 94% (Bendig et al., 2013; Chapman et al., 2014; Madec et al., 2017). Flying with more overlap is more time consuming but generates more images to capture every location, which Walter et al. (2018) reported to generate better correlations with ground measurements. Therefore, for the current experiment the overlap was selected to find a balance between good quality and efficiency.

The multirotor platform, Matrice 100 by DJI, was used to acquire imagery of 0.5 cm spatial resolution. The camera used was a SONY NEX 5, mounted on a gimbal beneath the drone. Multirotor UAVs are more suitable for small areas and are able to acquire higher resolution imagery, because their flights can be slower, allowing for higher image overlapp for succesful 3D model reconstructions.

The preferred flight conditions where clear sky before noon and with low wind, because shadows due to low sun angle and windy conditions are suspected to be detrimental for the quality of plant height extraction from 3D models generated from UAV (Brocks et al.,

2016; Brocks & Bareth, 2018). The ideal setting was planned to do the flight with platforms very closely in time. However, metheorological conditions and overlapp with other activities did not allow the ideal contitions in all the flights. A summary of the flight conditions for the two centimeter imagery can be found in APPENDIX A.

3.3.2.2 GEOREFERENCE

To have the data properly georeferenced, different sources where used and this is related to the third specific objective of the thesis. As a starting point, the imagery was geotagged with the navigation system inbuilt in the UAV. The multirotor system has an accuracy of five to ten meters. For the fixed wing platform, an RTK accuracy enhancement was in place by using a GNSS base station connected to the flight control computer which was correcting the UAV location during the flight. The base equipment was a Trimble R4 GPS receiver (Trimble, Sunnyvale, CA, USA) fixed in a known location with a bipod. The RTK enhanced UAV is expected to have an accuracy of one to three times the ground sampling distance, *i.e.* two to six centimeters in this case. Dall'Asta et al. (2017) suggested that the RTK correction possibly could replace the use of GCP to accurately georeference UAV imagery and proved that the RMSE achieved can be from two to ten cm (Benassi et al., 2017).

Additionally to the UAV GNSS data, a set of seven ground control points (GCP) was placed in the field to improve the alignment of the series of maps that would be produced during the cycle. They were made of a rectangular plastic frame painted black and white in a two by two chessboard pattern, supported by a vertical metal bar. The frames were in horizontal position at an approximate height of 1.5 m above ground to avoid being covered by the plants. The GCPs where distributed in the corners of the trial and randomly along it, to have them homogeneously arranged as Sanz-Ablanedo et al. (2018) suggested. To know the accurate location of the marks, they were previously measured in a GPS survey using the same equipment used for the RTK correction, but not at the same time.

3.3.3 PHOTOGRAMETRIC 3D RECONSTRUCTION: DSM & RGB MOSAIC

The photogrammetric reconstruction of the 3D model was performed using SFM algorithms using Pix4Dmapper software (Version 4.4.4). The individual imagery acquired by the UAV is analyzed with computer vision to find identifiable key points. Matches are found where a point can be seen in multiple images. Even though the imagery has already geotags on it, a bundle block adjustment is performed to optimize the location of the position of the UAV at the image capture instant. These multiple points of view allow for stereoscopic reconstruction of the imagery resulting in a cloud of points representing the observable surface. Several recent studies have used these techniques for successful 3D reconstructions using UAV (Bareth et al., 2016; Geipel et al., 2014; Brocks & Bareth, 2018); the software Pix4D was used because it was available in CIMMYT and it has been compared with other photogrammetric software giving similar horizontal results (Benassi et al., 2017).

In the next step, the point cloud is triangulated to generate a Digital Surface Model. The option "noise reduction" and "surface smooth: sharp" were used in the software as parameters, selecting it after several tests.

The resulting DSM is used in the orthorectification process of the original individual images. The perspective and lens distortions are corrected in each image by the software. The undistorted images are merged in their corresponding geographic space, thanks to the geolocation, providing a full coverage of the area of interest in one mosaic. This output image has a uniform scale and true horizontal distances can be measured in it.

Once the photogrammetric preprocessing of the images was performed, the generation of the processed outputs followed it as it can be seen on Figure 11.

In the image processing step, some quality issues where identified, and action was taken accordingly. For the two-centimeter images georeferenced with RTK, the image from the dates January seventh and 27th where discarded because they had a spatial location inaccuracy error due to the base station position and 3D reconstruction artifacts due to very high wind during flight, respectively. The two-cm imagery georeferenced with GCP (two-cm GCP) for the 27th of January was also discarded for the same reason. Finally, the

0.5 cm imagery for February 15th was discarded because of 3D reconstruction artifacts, but the reason of the error was not possible to identify.

3.3.4 CSM GENERATION

The 3D point cloud was computed based on the imagery using structure from motion algorithms with the photogrametric software Pix4Dmapper. The terrain was subtracted from the surface model to get the "height" surface of the trial in a raster form, *i.e.* subtract the DTM from the DSM to get the CSM. Previously, many studies generated the CSM by subtracting the DTM from the DSM succesfully (Geipel et al., 2014; De Souza et al., 2017; Bendig et al., 2013; Bareth et al., 2016), obtaining the DTM differently, *e.g.* getting the elevation from survey coordinates of the soil or extracting from the UAV data the lower elevation points. The terrain was generated interpolating random points of soil inside the trial corresponding to the top of the beds from the first image using the Inverse distance weighting (IDW) method based on the methodology followed by Brocks & Bareth (2018).

3.3.4.1 EXTRACTION OF PLANT HEIGHT AND CORRELATION WITH GROUND MEASUREMENTS

Based on the generated CSM, the estimation of the wheat plant height by plot was estimated using the following workflow. To extract the plant height, the unit of work was the raster subset inside the plot polygon, as in Figure 12. The plots polygon outlines where generated with the adequate proportions and identifier of the actual plots and the extraction area is separated from the plant cut zones .

Because a section of the plot was used in the destructive biomass sample to the north of each plot, a section of two meters length of the whole plot was selected to perform the extraction. Some manual adjustments where performed due to field samplings that were not following the standard location for sampling. An important remark can be taken from here: the HTP pipelines enable to process in a very automated way big amounts of

information, however the quality control and the verification of "From-Plan-to-Field" activities is crucial to have quality data.
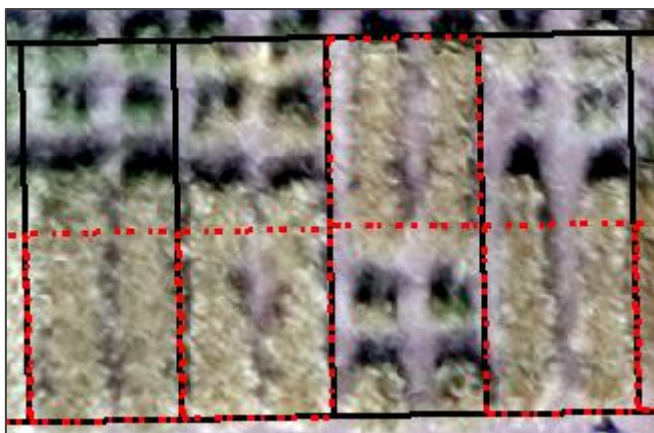
Figure 12. Example of plot polygon (black outline) with double bed and image extraction area (red dotted outline).

Other studies reported plant height extraction methods such as the mean of the pixels in the area of interest (De Souza et al., 2017), the 99th percentil (Holman et al., 2016) or the highest pixel value inside each individual area of interest (De Castro et al., 2018). The plant height was selected as the 99.5% percentil (Madec et al., 2017) of the pixels inside each plot because it was proven that it gives the best results compared to other percentiles. The extraction zone of each plot was buffered 15 cm to avoid soil and borders as done by Holman et al. (2016) and Geipel et al. (2014). The representation of the buffer zone is in Figure 13 where the extraction zone in yellow is centered on the vegetation area.

The software used was R with the packages "raster" (Hijmans, 2017) and "rgdal" (Bivand, Keitt, & Rowlingson, 2018) to open the images and to open the plot polygons, respectively. R programming language has been used for data processing in several recent publications (Geipel et al., 2014; Crain et al., 2016; Madec et al., 2017; Rutkoski et al., 2016).
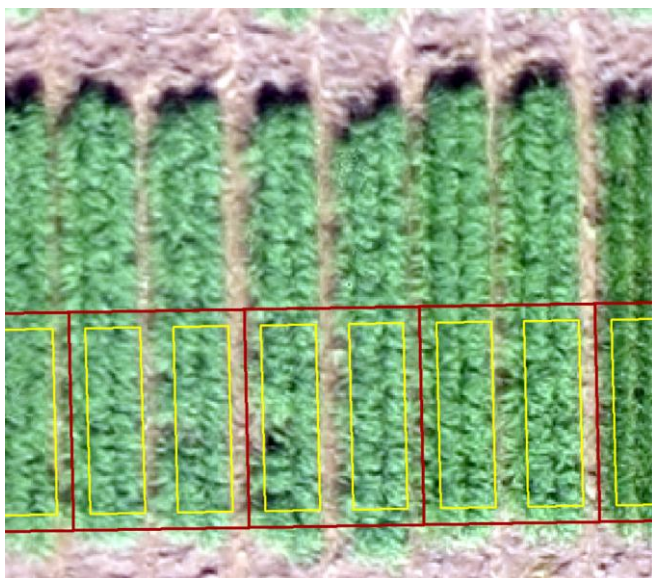
Figure 13. Buffer of 15 cm to extract the plant height from the CSM. The red outline is the plot polygon and the buffer for each bed is in a yellow outline.

Pearson's correlation was used to assess the relationship between the remote and proximal data as done by Chapman et al. (2014), using the RMSE as a measure of the accuracy as done by Harwin & Lucieer (2012). The R packages used were "PerformanceAnalytics" (Peterson & Carl, 2013) and "Metrics" (Frasco, 2018), to perform the correlation charts and calculate the RMSE, respectively. The field manual measurements were compared to the drone remote data that was captured the same day or a maximum of two days after or before them. Due to practical issues which prevented drone data capture, some plots do not have a corresponding remote measurement at certain stages. A summary of the total number of matching samples at each stage and image resolution can be seen in Table 1.

Table 1. Number of matching plant height observations between manual and remote data.

Stage	measurement	Number of matching observations	
		Two-cm imagery	0.5-cm imagery
Maturity	Height	93	19
Anthesis	Height	30	16
Booting	Height	29	74

3.3.4.2 EXTRACTION OF VOLUME AND CORRELATION WITH GROUND MEASUREMENTS

The volume of the plot will be the proxy measure to estimate the plant biomass. To obtain the volume from the 3D model, the DSM and the DTM where used to delimit the upper and lower limits of the reconstructed plant volume, respectively. Additionally, to fully delimit the 3D plot to be considered, the Greenness Index (Wenzhu et al., 2015) was used to select the horizontal extent to consider, functioning as a binary mask as suggested by Madec et al. (2017) to improve the volume estimations, because otherwise the different ground coverage for the plots is not considered. Schirrmann et al. (2016) used a similar approach to discriminate soil and vegetation from the color, but they used the a-vector in the LAB color space. This greenex index was selected because it showed robust results differenciating the green in different field light and soil condition. However it was adapted to the needs of the experiment, because the different color between early and late stages did not all provide a satisfactory result with the default parameters, just in the green early stages. To get the adapted parameters for the Greeness index filter, the 0.05% and 99.5% percentil was used as minimum and maximum values for each date in the hue, saturation and value (HSV) channels to calculate the index. An example of the results can be seen in Figure 14, where the soil is removed and the vegetation kept. This filter shows where the cultivars in the different plots have varying ground cover. The greenness index calculation

step of deleting objects smaller than 100 pixels was not used because there are no objects in the images other than wheat as GCP are removed with the filter and do not fall inside the plot polygons.

The R packages "raster" (Hijmans, 2017), "grDevices" (R Core Team & contributors worldwide, 2017) and "rgdal" (Bivand et al., 2018) were necessary to open the images, convert from the RGB to HSV color spaces and to open the plot polygons, respectively.

To process the imagery of the 0.5 cm resolution, mosaics were split by the half and the greenness Index calculation done separately to each part. After processing they were merged together again to continue with the extraction process. This was necessary because the file was processed erroneously in the part of the greenness filter code when it worked with the HSV functions. The source of the problem was the big file size of these very high-resolution imagery.
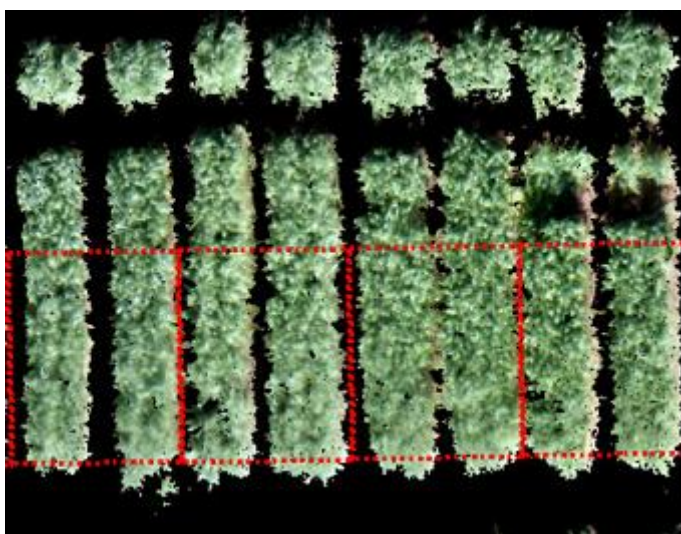
Figure 14. Example of the greenness filter applied; the removed soil is in black. The plot area of interest in dotted red line.

To compute the reconstructed volume of a plot V_{3D}, the DTM elevation was subtracted from the DSM to generate a difference surface H_{3D} that represents the height at each point. Then, within every plot polygon, the sum of each H_{3D} pixel that corresponds to the class "plant" in the HSV tree decision in the greenness index filter was multiplied by the pixel area, giving the reconstructed volume V_{3D} of each plot. The volume computation summing

the plot's pixel CSM height multiplied by the pixel area is similar than the methodology followed by De Castro et al. (2018).

After calculating the volume, Pearson correlation was used to correlate plant biomass measured manually with plot volume as predictors variable. RMSE was used as accuracy measurement. The observations with matching dates from the two traits were used, giving a two day tolerance of difference in the capture date. There were a varying number of observations for the different growth stages when some field measurements where not matched with the remote measurements, as can be seen on Table 2.

Table 2. Number of matching biomass manual observations between and CSM volume dates.

Stage	measurement	Number of matching observations	
		Two-cm imagery	0.5-cm imagery
Maturity	Biomass	296	77
Anthesis	Biomass	80	82
Booting	Biomass	85	222

3.4 IDENTIFICATION OF SUITABLE RESOLUTION AND GEOREFERENCING METHOD

To assess the most suitable resolution and georeferencing method, data were georeferenced using two different paths: ground control points or direct GNSS diferential correction on the imagery geotag. The results were compared to search for significant differences in the plant height and biomass estimations, in comparison with ground truth data, as well as the shift distance between both methods.

Root Mean Square Error (RMSE) metric was used to evaluate the accuracy of the two georeferencing approaches compared to the location of the GCP (Harwin & Lucieer, 2012).

The locations of the center of the GCPs marks in each image were compared to the original measured coordinates of the GCP, the and residuals were used to calculate the RMSE.

4 RESULTS AND DISCUSSION

4.1 RESULTS

The results of the comparisons are presented here for the two spatial resolution datasets and the two different georeferencing methods for the different crop growth stages. The stages of analysis for the plant height measurements were anthesis and for the date of March eighth. The manual plant height was also collected at booting, but the records were lost, and it was impossible to make the comparison for that stage.

For biomass vs volume comparison, the stages analyzed where booting, anthesis and maturity. It is worth to remark the varying number of samples at each different comparison because the drone data could not be acquired for every field measurement date, considering that the developmental stages for the different varieties occurred at different days.

The next map in Figure 15 shows the location of the plant-height sampled plots in the repetition one and two used for the analysis. The plant height CSM from March eighth is showed with the RGB image as base map. The biomass was sampled in all the plots from the replicate one and two.
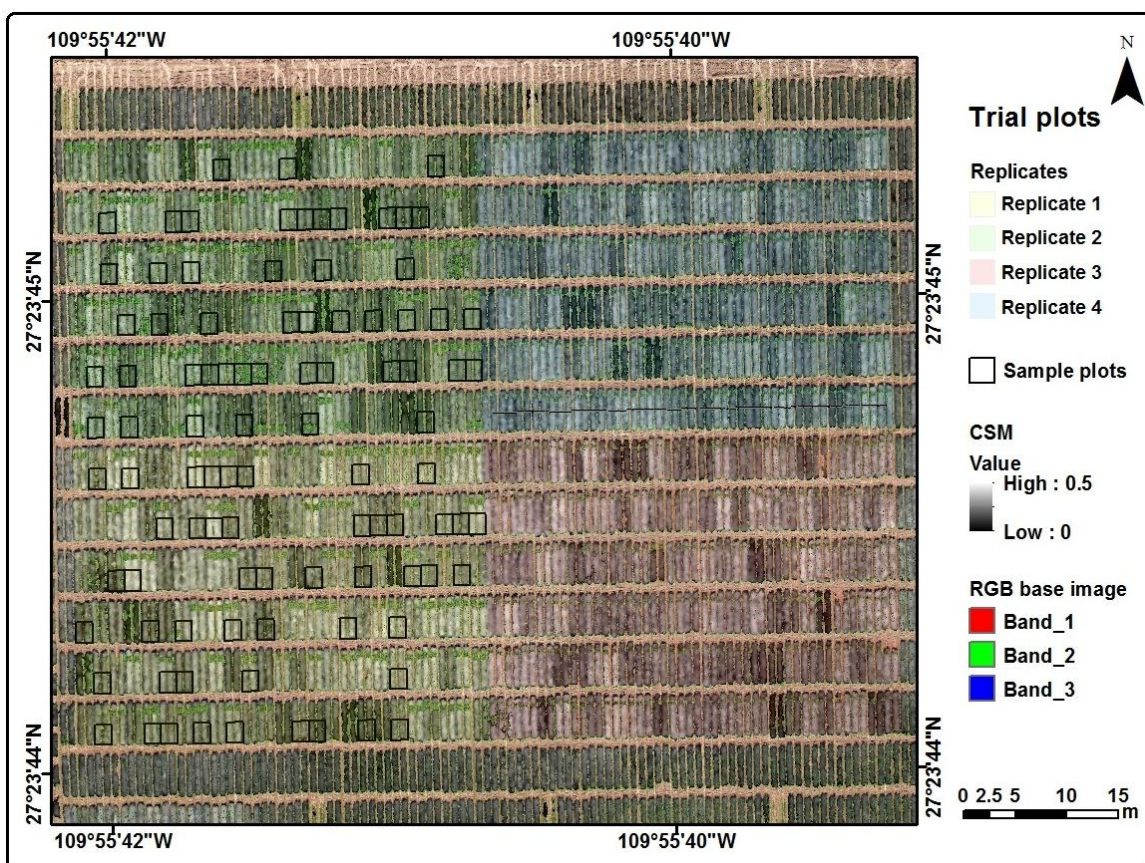
Figure 15. Location of analyzed plots in the trial for plant height comparison.

4.1.1 ESTIMATION OF PLANT HEIGHT

Results obtained for the linear regression for the data obtained from the two-centimeter imagery georeferenced with GCPs, the Pearson correlation's coefficient (R), with field manual measurements in the anthesis stage and at the eight of March is presented in the Table 3 and the graphics of the correlation is presented in Figure 16. The highest correlation is 0.87 for the eight of March where the points of the graph correspond to a good correlation. This say was when the data was collected the same day. Anthesis stage showed an R = 0.55 and RMSE almost double than the eight of March, but the number of samples was almost a third because of the offset of sampling dates. The graph for this stage shows more dispersion of the points, related to the lower correlation.

Table 3. Plant height correlation coefficients of the two-centimeter imagery georeferenced with GCP.

Plant height: Two-centimeter imagery georeferenced with GCP			
Growth stage	R	RMSE	n
Anthesis	0.55 **	0.441	30
March eighth	0.87 ***	0.197	93
Maturity	0.60 ***	0.311	93

The significance levels are showed with stars as follows: *** = 0.001, **=0.01
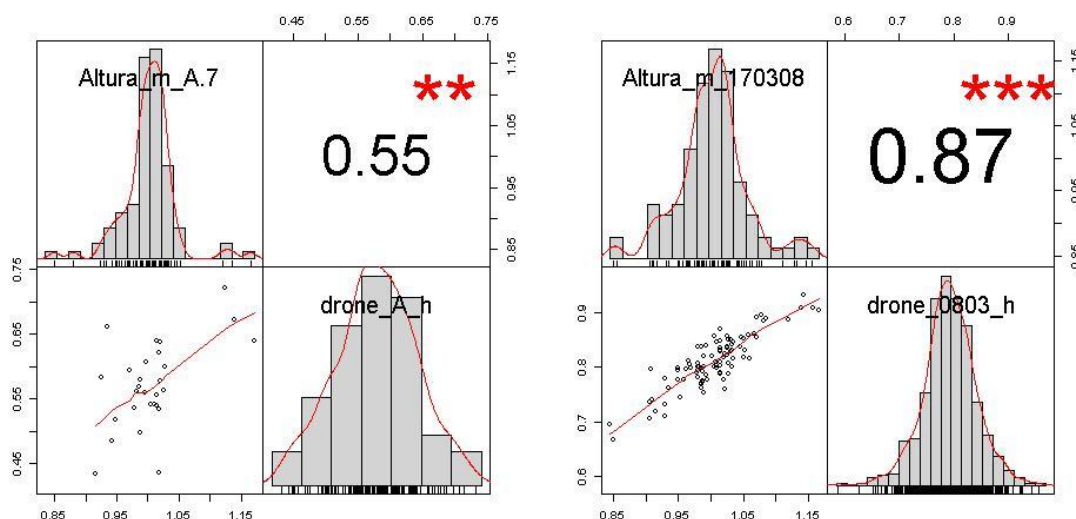
Figure 16. Correlation of the two-centimeter imagery georeferenced with GCP: manual height measurements vs imagery at anthesis stage (left) and for the eighth of March (right).

For the two-centimeter resolution georeferenced directly with RTK (two-cm RTK), the Pearson correlation's coefficient (R) in the comparison with field manual measurements in the anthesis stage is presented in Table 4 and the graphics of the correlation is presented in Figure 17. Here again the best correlation was in the eight of March (R = 0.85) with a significance level of 0.001. The results are very similar for to the two-cm GCP data. The anthesis sampling gave an R = 0.52 and the RMSE is almost the double than the maturity stage, but the number of samples was one third.

Table 4. Plant height correlation coefficients of the two-centimeter imagery georeferenced with RTK.

Plant height: Two-centimeter imagery georeferenced with RTK			
Growth stage	R	RMSE	samples
Anthesis	0.52 **	0.385	30
March eighth	0.85 ***	0.118	93
Maturity	0.68 ***	0.177	93

The significance levels are showed with stars as follows: *** = 0.001, **=0.01
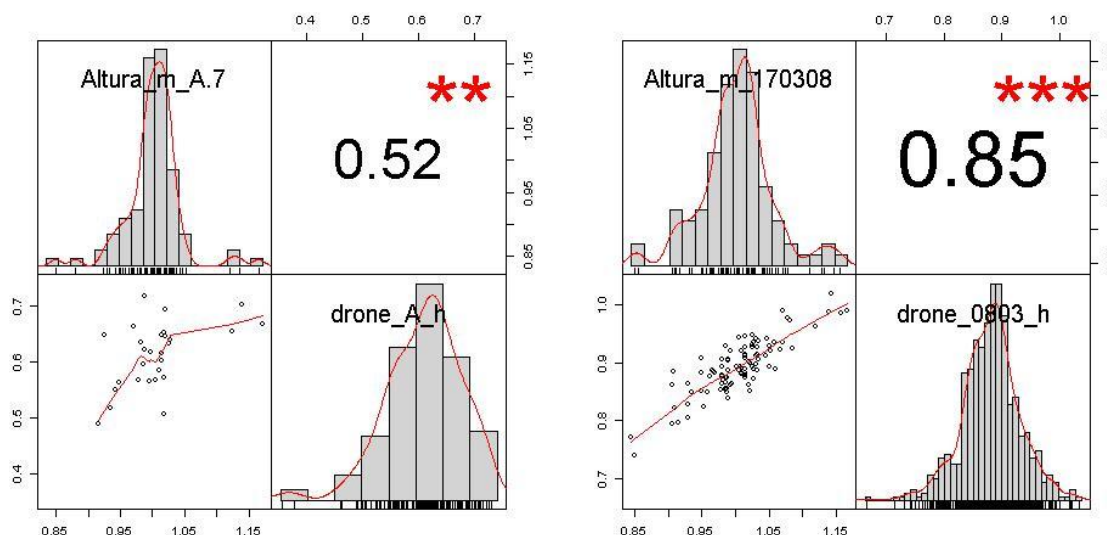
Figure 17. Correlation of height measurements in the anthesis stage (left) and in the eighth of March (right) for the two-cm imagery georeferenced directly with RTK.

As per additional comparison, the manual height measured at the anthesis stage was compared with the measurements obtained at the maturity stage with the two-centimeter imagery. This had the intention of exploring the statement that in the anthesis the maximum plant growth is reached (Madec et al., 2017). The correlation found were 0.6 and 0.68 for the dataset georeferenced with GCP and RTK, respectively as can be seen on Figure 18. In the correlation graphs the points appear well aligned in general and especially in the extremes, however some disperse points are present too.
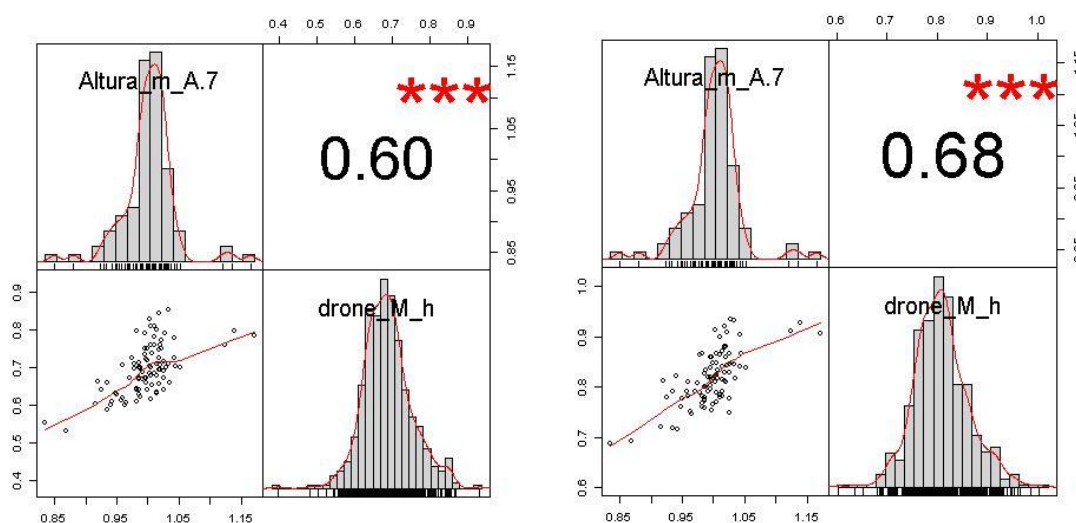
Figure 18. Correlation of height measured manually in anthesis and with the drone at maturity for the two-centimeter imagery georeferenced with GCP (left) and directly with RTK (right).

Following the same procedure, the height extracted from the 0.5-cm resolution $CSM_{0.5cm}$ was compared with the ground measurements. This were only georeferenced with GCP because the platform did not have DGPS capabilities. Results are presented below in the

Table 5 and the graphics of the correlation is presented in Figure 19. Consistently with the two-cm imagery, the data for March eight showed the higher correlation while maintaining approximately the same RMSE. However, samples for anthesis and maturity stages were considerably lower. Results for anthesis stage show still a relatively high R = 0.61, however with a much lower significance level of 0.1 compared to results above with more samples. An outstanding change was the very low correlation in the maturity stage, which even shows a negative sign.

Table 5. Plant height correlation coefficients of the 0.5-cm imagery georeferenced with GCP.

Plant height: 0.5-cm imagery georeferenced with GCP			
Growth stage	R	RMSE	samples
Anthesis	0.61 *	0.407	16
March eighth	0.57 ***	0.171	93
Maturity	-0.25	0.148	19

The significance levels are showed with stars as follows: *** = 0.001, **=0.01, *=0.1
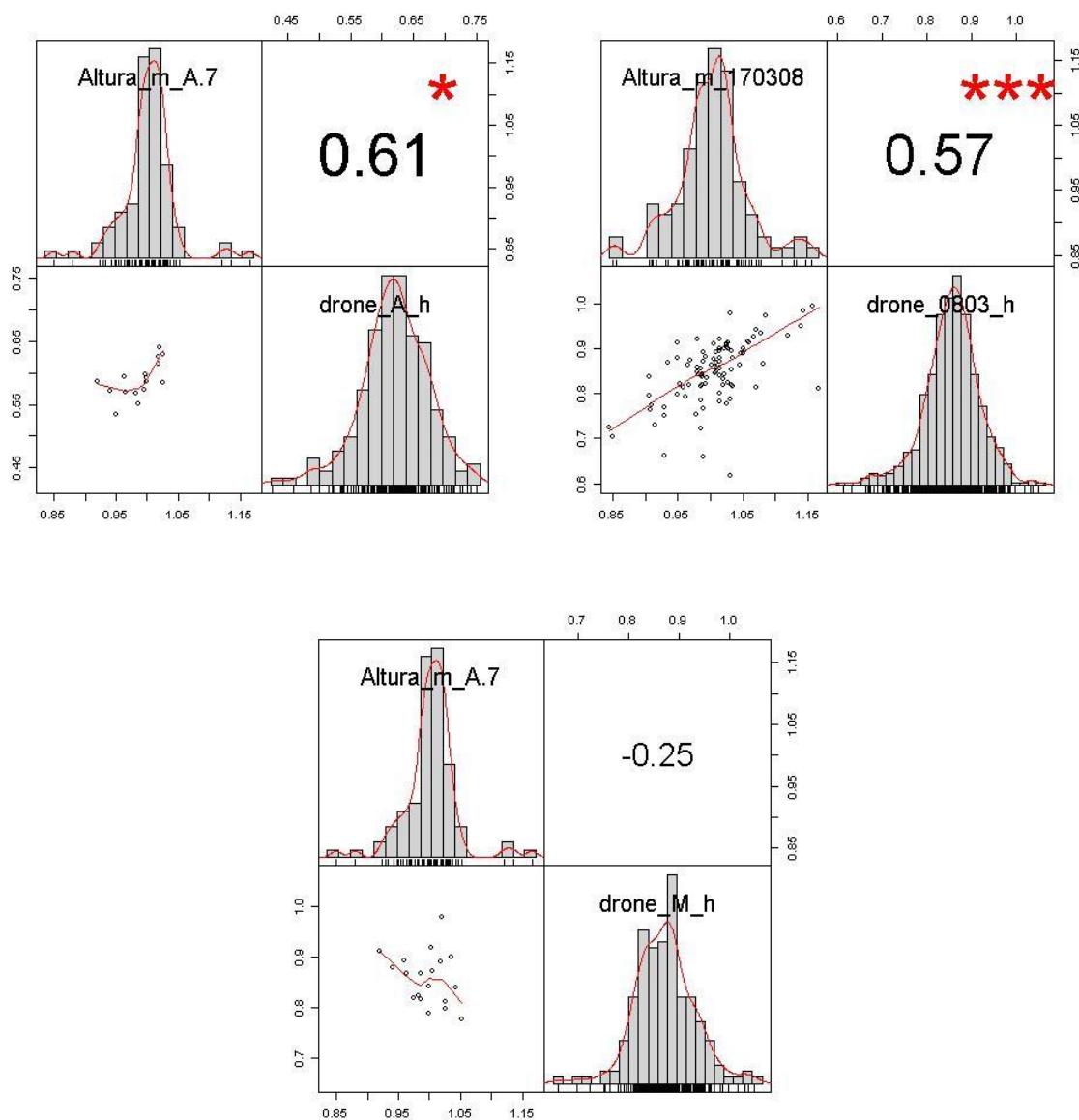
Figure 19. Correlation of height measured manually in anthesis (left) and on March eighth (right) with the drone for the half-centimeter imagery.

The 0.5-centimeter imagery did not present relevant correlation in the comparison between the manual height measured at the anthesis stage vs the drone measurements obtained at the maturity stage. However, the drone data acquisition dates corresponded to a very limited number of plots in that stage (n=19).

4.1.2 ESTIMATION OF BIOMASS

The variable for the estimation of the biomass was the sample plot volume for the different image resolutions and georeferencing method. The volume was calculated using the CSM for the height and the greenness VI to obtain the area covered in each plot, multiplied to calculate the volume. The analyzed growth stages where booting, anthesis and plant maturity. In general, anthesis and maturity stage present varying levels of moderate correlation in the different resolutions and georeferencing methods, but booting stage shows a negligible correlation in all cases.

Results of the linear regressions comparing the 3D computed plot volume with the biomass samplings for the two-centimeter imagery georeferenced with GCP are showed in Table 6 and the graphics of the correlation is presented in Figure 20. The number of samples available for the biomass comparisons was reduced for the two-cm imagery due to field technical issues, only at maturity stage almost all the samples were used for the correlations. Anthesis and maturity stage show a mild correlation of 0.29 and 0.3, respectively; they have a RMSE in the range of 0.4 and the significance level of 0.1 vs 0.001, respectively.

Table 6. Plot volume correlation coefficients of the two-centimeter imagery georeferenced with GCP.

Plot volume: Two-centimeter imagery georeferenced with GCP			
Growth stage	R	RMSE	samples
Booting	0.065	0.168	85
Anthesis	0.29 *	0.488	80
Maturity	0.30 ***	0.415	296

The significance levels are showed with stars as follows: *** = 0.001, *=0.1
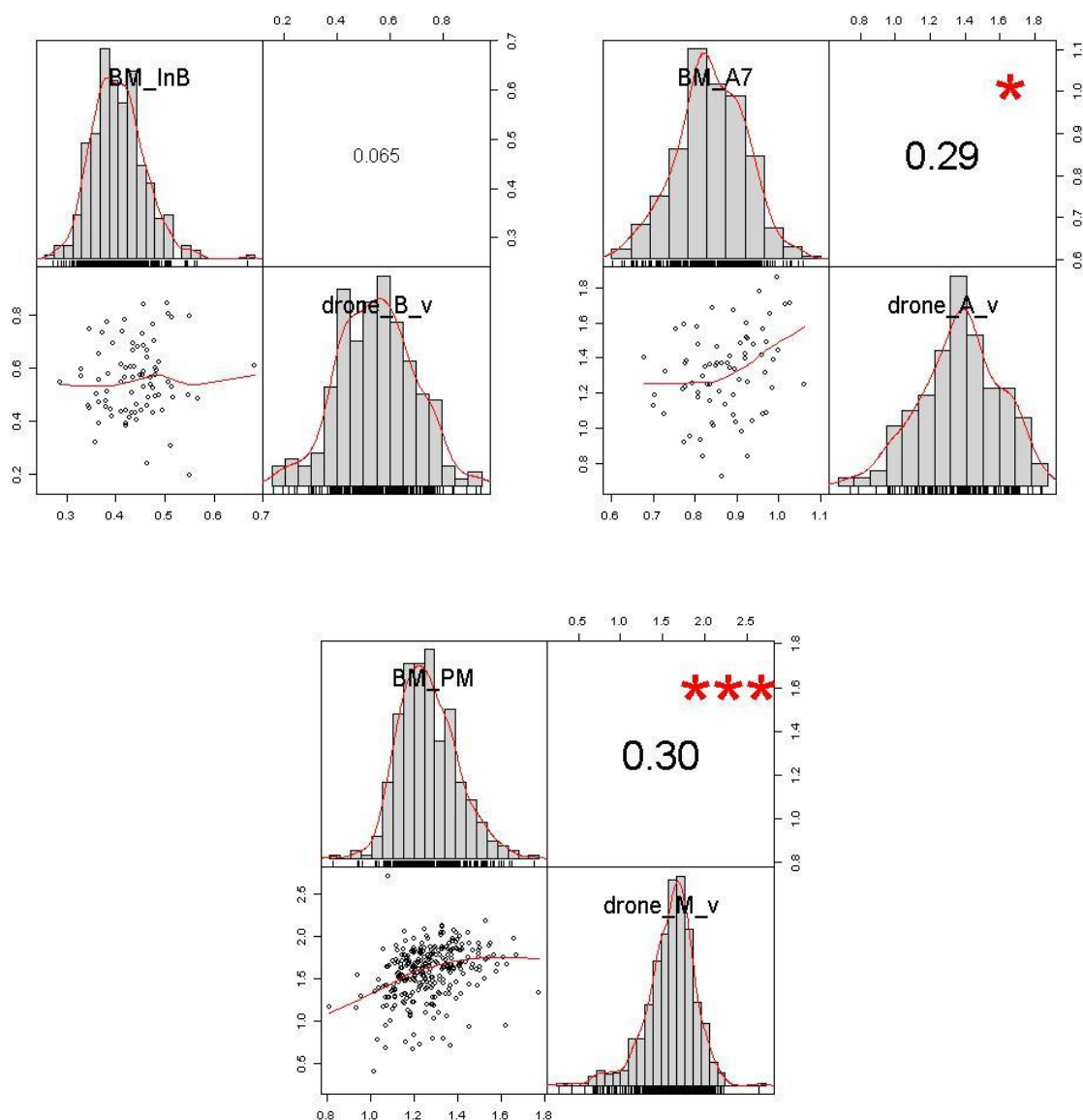
Figure 20. Correlation of biomass measured and plot volume estimated with the drone at booting, anthesis and maturity for the two-centimeter imagery georeferenced with GCP.

The values for the correlations of plot volume and biomass samples for the two-cm imagery georeferenced directly with RTK at the evaluated staged are presented in Table 7 and the graphics are in the Figure 21. The three graphs show very disperse points, which is reflected in the low correlation values, but booting stage shows no tendency of agreement between biomass and estimated volume. The values of correlation and RMSE are very similar to the two-cm GCP method above: in anthesis stage, the correlation is 0.03 higher in the RTK

method and with a significance level one order of magnitude lower, but the RMSE 0.04 higher.

Table 7. Plot volume correlation coefficients of the two-centimeter imagery georeferenced with RTK.

Plot volume: Two-centimeter imagery georeferenced with RTK			
Growth stage	R	RMSE	samples
Booting	0.044	0.143	85
Anthesis	0.32 **	0.529	80
Maturity	0.29 ***	0.78	296

The significance levels are showed with stars as follows: *** = 0.001, **=0.01
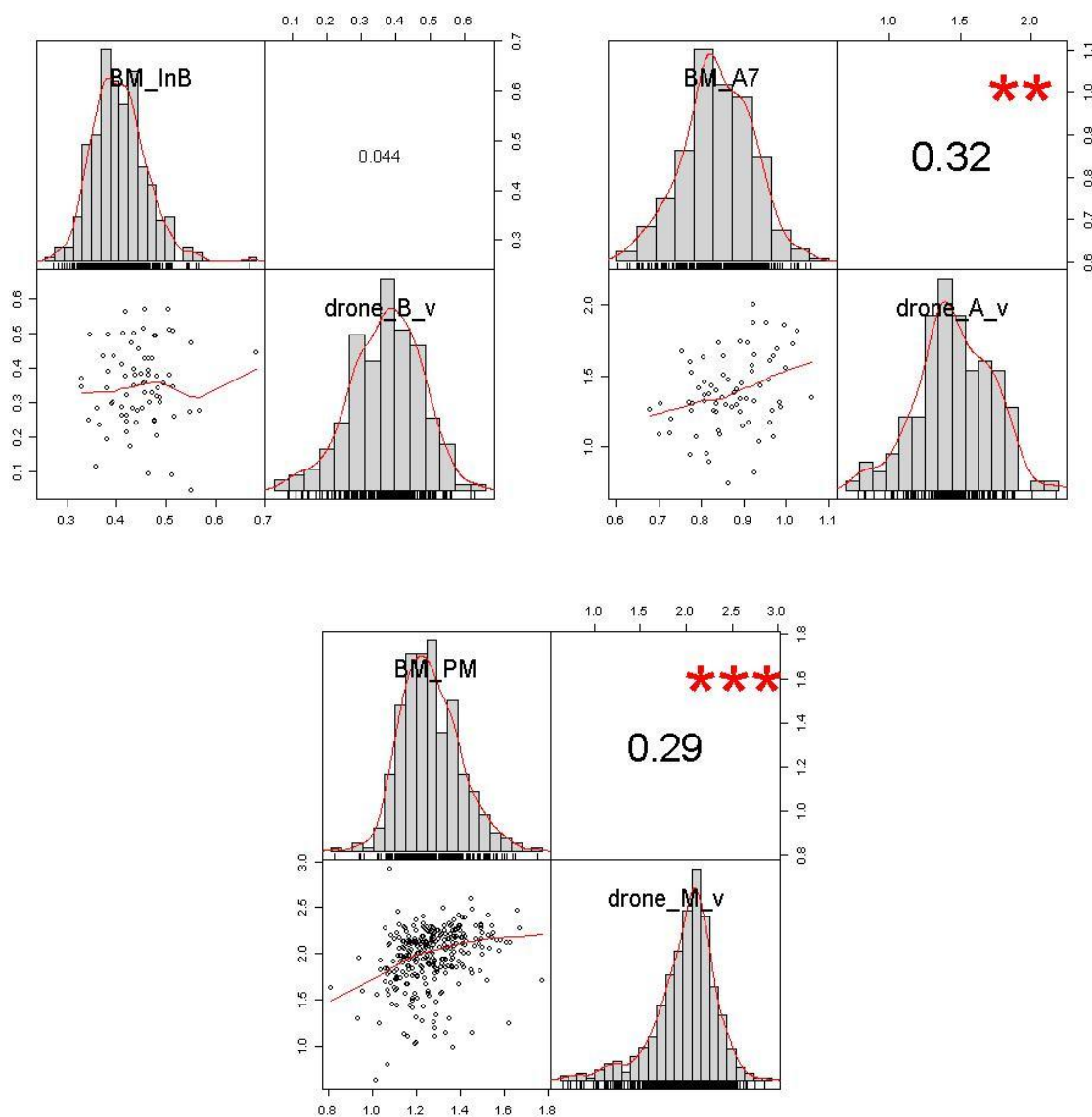
Figure 21. Correlation of biomass measured and plot volume estimated with the drone at booting, anthesis and maturity for the two-centimeter imagery georeferenced with RTK.

The results for the plot volume and biomass comparisons for the model generated with 0.5-cm resolution imagery are in Table 8 and the graphics of the correlations are in Figure 22, showing the three evaluated stages. The imagery at this resolution was only georeferenced using GCP. The result in the biomass stage show no correlation with a negative sign (R = -0.01) without statistical significance. In this stage a comprehensive number of samples was used. In anthesis a mild correlation is present (R = 0.4) with a significance level of 0.001, despite the reduced number of samples available.

Table 8. Plot volume correlation coefficients of the Half-centimeter imagery georeferenced with GCP.

Plot volume: Half-centimeter imagery georeferenced with GCP			
Growth stage	R	RMSE	samples
Booting	-0.01	0.512	222
Anthesis	0.40 ***	0.408	82
Maturity	0.22	0.797	77

The significance levels are showed with stars as follows: *** = 0.001
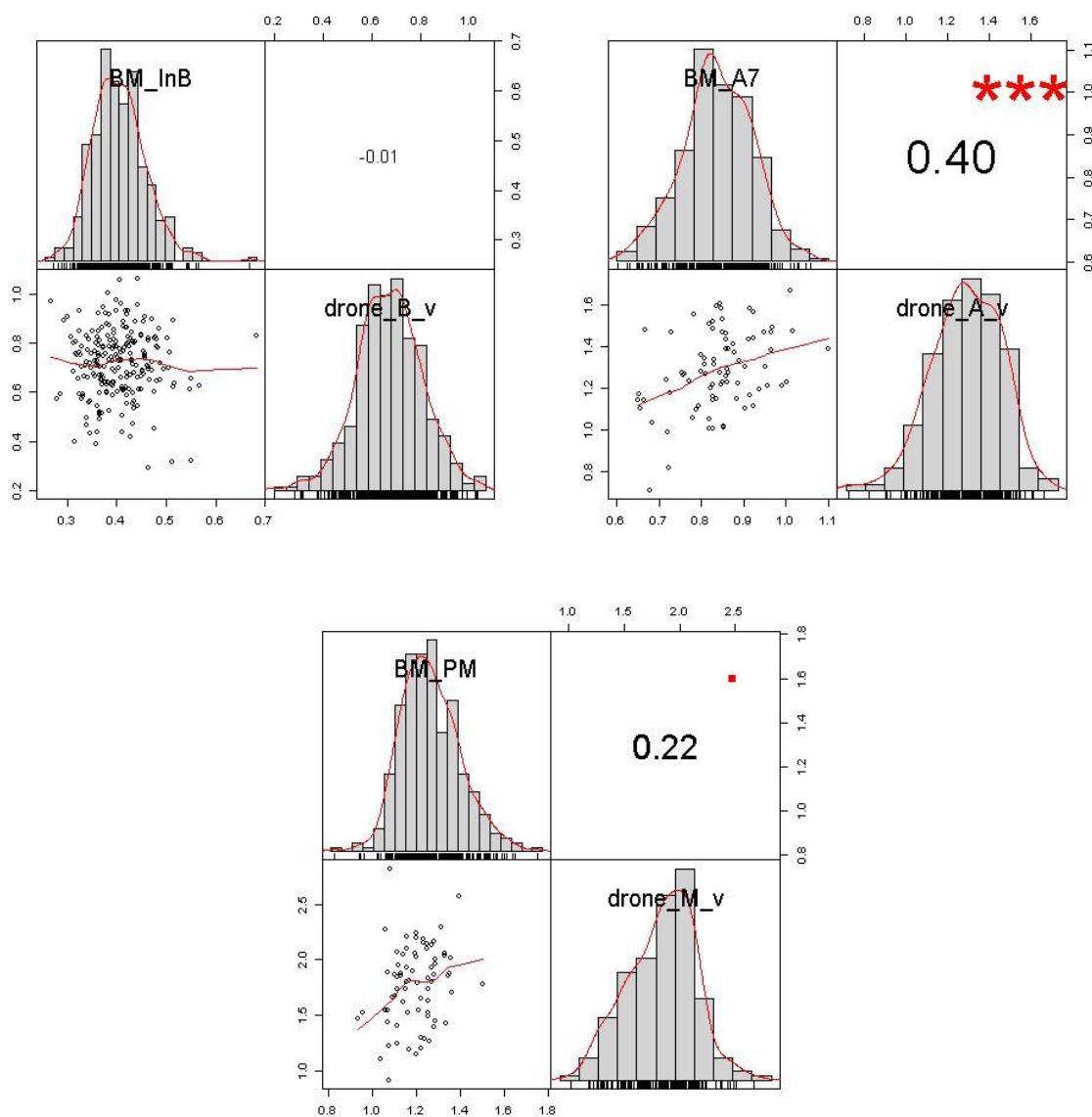
Figure 22. Correlation of biomass measured and plot volume estimated with the drone at booting (InB), anthesis (A7) and maturity (PM) for the Half-centimeter imagery georeferenced with GCP.

The data showed practically inexistent correlation between the estimated volume and the biomass at booting stage from the imagery for all the resolution and georeferencing methods. In the anthesis stage, a correlation between 0.29 and 0.4 was found across all methods; as well as in the maturity stage being in the range of 0.22 to 0.3.

4.1.3 IDENTIFICATION OF SUITABLE RESOLUTION AND GEOREFERENCING METHOD

To compare the effects in the results of the different georeferencing and the different resolution imagery, the RMSE values were compared. First the tables of the GCPs residuals from the image corresponding to the day 13th of February are shown for all the methods. Then the RMSE in X and Y are shown.

The Table 12, Table 13 and Table 14 in the APPENDIX B show the image location of the center of the GCP marks, the measured GCP location and the residuals between them for the image from February 13 for the two-cm GCP, two-cm RTK and 0.5-cm GCP imagery, respectively. Table 9 presents the RMSE of the two-cm GCP, two-cm RTK image and the 0.5-cm GCP image. The first comparison is two-cm GCP versus two-cm RTK: accuracy in X was almost four times better with the GCP method, but for the Y component the difference was only 0.006. Results between the two-cm GCP method with the 0.5-cm GCP was very tight: RMSE in X was better for the 0.5-cm by 0.009, but worse in the Y component by 0.007.

Table 9. Results of the RMSE in the three methods compared in the image of February 13.

Image, date February 13	RMSE X	RMSE Y
Two-cm GCP	0.020	0.017
Two-cm RTK	0.086	0.023
0.5-cm GCP	0.011	0.024

Additionally, the accuracy of all the dates for the two-cm RTK imagery was measured. The RMSE per GCP is shown in Table 15, in the APPENDIX B. The average RMSE in X is 0.065 m and 0.034 m in Y. The map in Figure 23 shows the RMSE exaggerated one hundred times. There is variation in the magnitude of the error across points and between the X and Y component. This could lead to suspect in measurements errors during the survey. However, a tendency for a bigger error in the X component is visible.
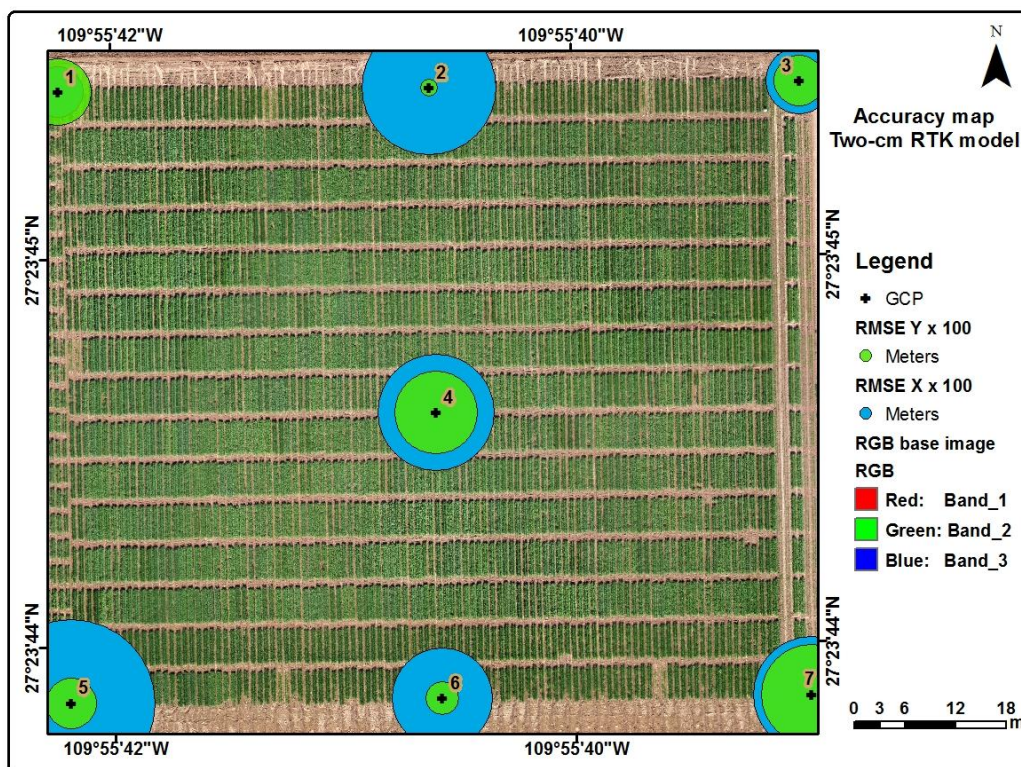
Figure 23. Map of the average RMSE error per GCP for the two-cm RTK imagery

To compare the effect of resolution on the estimations of height and biomass, the RMSE and R of the correlations was used, the results can be seen in the Table 10. The colors of the cells of R and RMSE are relative to the comparison between methods for each individual stage and trait. For plant height, the results in the 3 methods follows the same trend for the stages, except for maturity for the 0.5-cm GCP. For the two-cm imagery, in anthesis and March eight, the GCP method showed a correlation 0.02-0.03 better than the RTK, but an RMSE 0.056-0.079 higher; for the maturity stage, RMSE and R were better with the RTK. The 0.5-cm results compared to the two-cm GCP had a lower correlation and the RMSE was in the same range as the two-cm imagery.

For the biomass comparison, at booting, the higher correlation was 0.065 at the two-cm GCP, but the two-cm RTK imagery presented the lower RMSE (0.143), while the 0.5-cm GCP presented the higher RMSE (0.512). For anthesis, the 0.5-cm GCP imagery showed the

higher correlation of 0.40 and for maturity it was the two-cm GCP with R= 0.30. The RTK method and the 0.5-cm GCP presented more frequently higher RMSE than the two-cm GCP.

Table 10. Results of the accuracy measurements for the estimations for all the methods

Imagery	Trait	Growth stage	R	RMSE	n
two-cm GCP	Height	Anthesis	0.55	0.441	30
two-cm GCP	Height	March eighth	0.87	0.197	93
two-cm GCP	Height	Maturity	0.60	0.311	93
two-cm RTK	Height	Anthesis	0.52	0.385	30
two-cm RTK	Height	March eighth	0.85	0.118	93
two-cm RTK	Height	Maturity	0.68	0.177	93
0.5-cm GCP	Height	Anthesis	0.61	0.407	16
0.5-cm GCP	Height	March eighth	0.57	0.171	93
0.5-cm GCP	Height	Maturity	-0.25	0.148	19
two-cm GCP	Biomass	Booting	0.07	0.168	85
two-cm GCP	Biomass	Anthesis	0.29	0.488	80
two-cm GCP	Biomass	Maturity	0.30	0.415	296
two-cm RTK	Biomass	Booting	0.04	0.143	85
two-cm RTK	Biomass	Anthesis	0.32	0.529	80
two-cm RTK	Biomass	Maturity	0.29	0.780	296
0.5-cm GCP	Biomass	Booting	-0.01	0.512	222
0.5-cm GCP	Biomass	Anthesis	0.40	0.408	82
0.5-cm GCP	Biomass	Maturity	0.22	0.797	77

4.2 ANALYSIS OF RESULTS

4.2.1 ESTIMATION OF PLANT HEIGHT

For all the resolutions and georeferencing methods, the most outstanding correlation was for the plant height on the eighth of March, when measurements where made all in the same day for all the sampling plots, giving a R from 0.57 to 0.85. Next remarkable stage was maturity. As previously documented in the literature, the plant height obtained from the CSM appears to be underestimated compared to the manual measurements, given the ranges of the data (De Souza et al., 2017), possibly related to the difficulty of the SFM

techniques to reconstruct the small parts on top of the plant, *i.e.* spikes, when the image resolution is approximately the same size as them (Madec et al., 2017). In Figure 24 an example height profile of the date March eight is presented, comparing the two-cm GCP, two-cm RTK and 0.5-cm imagery with the field measurements. For some plots, all the measurements are very close, *e.g.* at the end of the profile, but in others the measurements are more disperse, *e.g.* at the beginning of the profile, however in general they show the same trend. The vertical offset between the two-cm GCP and the two-cm RTK models is related to the georeferencing accuracy. The map shows the location of the profile in the experiment. As a note, there were small issues in the 3D reconstruction in the middle left-most part of the 0.5-cm mosaic for this date.

Additionally, it could be seen that the plant height in the anthesis stage correlates very well with the height of the mature plants, aligning to the affirmation that the flowering stage can be practically considered the peak for crop height growth (Madec et al., 2017).
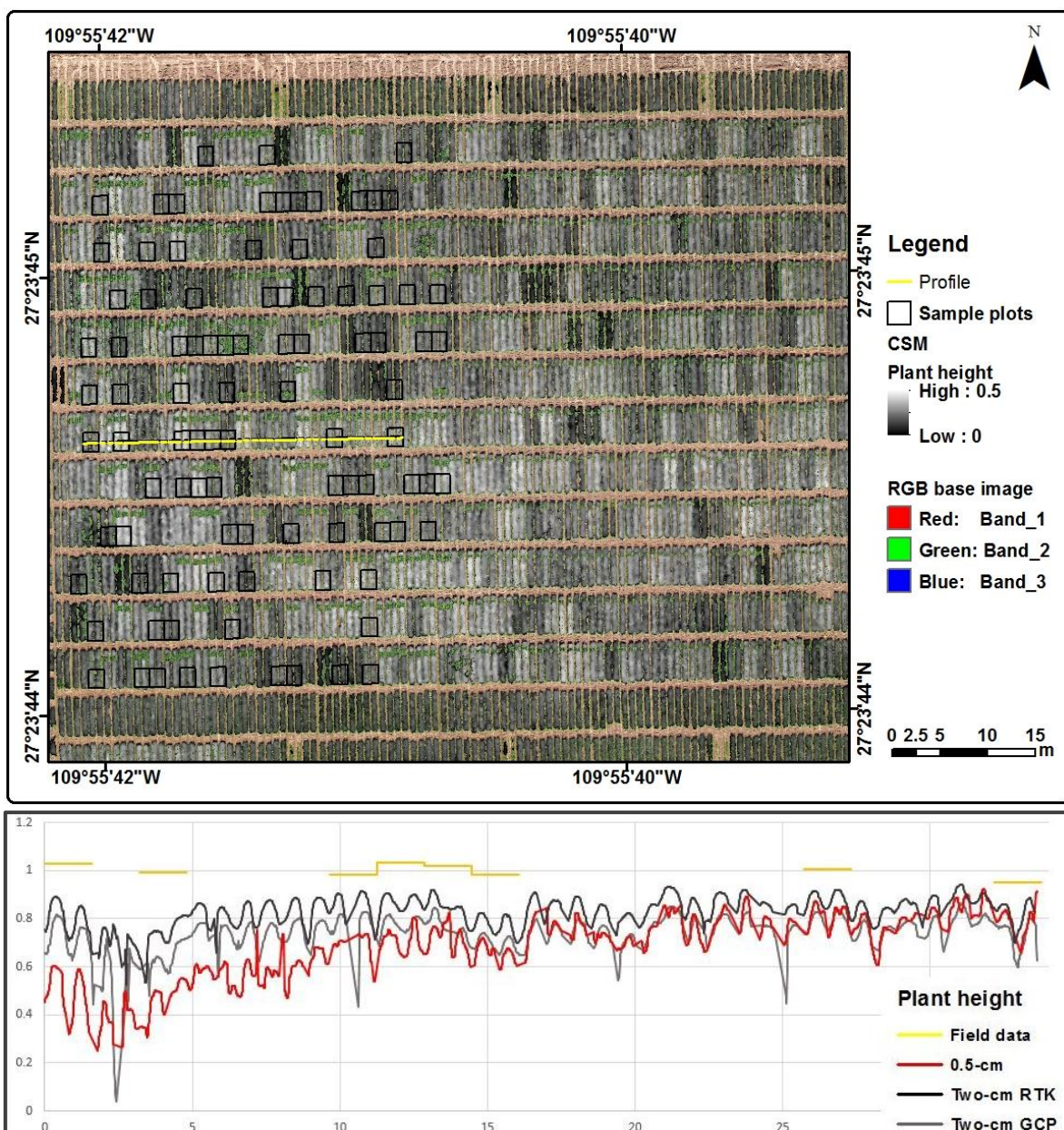
Figure 24. Plant height profile

Comparing the indirectly estimated height (from UAV) to a directly measured one (with ruler) that can have low representativity of the crop (Bendig et al., 2014), due to very few samples that are practical to make, the method has great oportunities for improvement. An alternative to validate height estimated from UAV 3D models could be the well documented LIDAR terrestrial scanning. Once that the validation is complete, the time saved in samplings could allow for more intensive work.

As in Bareth et al. (2016), different trends in the correlations of estimated height versus reference measured data at different stages have been observed. A great drawback of the approach followed in this study was that only one stage was compared at a time, being able to improve if all the stages were combined. As well, the missing data for the booting stage for height did not allow for comparisons in all the stages, as well as the many plots that did not have remote data in the day corresponding to certain stages.

The implications in difference in the "height" concept used in phenotyping trial measurements and what can be measured remotely should be analytically considered. Given the fact that in field measurements the straight distance from the soil to the upper part of the spike along the plant shoot is considered, and in UAV photogrammetry reconstruction the height would be computed vertically from the soil surface, disregarding any inclination of the plant.

For the data capture, more emphasis should be given to the importance of the wind condition for an accurate 3D reconstruction. Weather is a factor in agriculture that can not be controlled, but certain procedures could mitigate its negative effect. For example, flying earlier in the day in the CENEB station typically allows to fly in lower wind conditions compared to the afternoon. However, since sufficient light conditions are also needed, there is no perfect answer. More research should be done to assess the influence of wind and determine if there is any acceptable limit that would allow reliable results or indicate that data should not be acquired. As well, the flight plan for earlier in the season was adjusted in the later flights to cover several times the field to acquire more imagery for the two-centimeter imagery, giving an uneven number of images along the season.

4.2.2 ESTIMATION OF BIOMASS

The obtained results show a moderate-low correlation of biomass with volume in all the datasets, and it varies in the different growth stages as can be seen in Table 6, Table 7 and Table 8. The best correlations are shown in the anthesis and maturity stages (R between 0.29 and 0.40). On the contrary, no correlation was present in the booting stage. However,

in previous studies it was perceived that the correlation for individual stages was lower than compared to the use of all the growing cycle data (Madec et al., 2017; Brocks & Bareth, 2018).

The method for calculating the volume can improve in the greenness filter algorithm, which may lead to a better estimation of biomass from it. Different methods for filtering the crop pixels can be tested and assessed, *e.g.* simply using a plot buffer to remove boundary effect (Bendig et al., 2013) or using object-based image analysis classification to select plant pixels (De Castro et al., 2018). This was not the main focus of the work, but it can be a very important point to be considered for future work.

In Walter et al. (2018), higher correlations were found between estimated volume and measured biomass. A main issue may be that they used higher spatial resolution, because the imagery was taken from the field in front of the plots and from all angles of every plot. This work has less image overlap, and spatial resolution compared to it. The UAV + RTK method of acquisition is being explored to be a way to save time in the image acquisition and processing stages.

The remark mentioned in the literature that finds that plant height measurements and above ground biomass to show better overall correlations if all the stages are considered, rather than individual stages or dates is partially confirmed in the current analysis. The individual stage correlation is moderately low to high. Looking at the ranges of the measurements in all the stages, it can be expected that they will describe better the correlation of the remote sensing estimations compared to the field direct measurements if they are used together.

4.2.3 IDENTIFICATION OF SUITABLE RESOLUTION AND GEOREFERENCING METHOD

Regarding location accuracy, all imagery was accurate enough to fit every plot in the image above the corresponding plot polygon. The GCP method gave slightly better results than the RTK, but it requires considerably more field work and user intervention in the

processing. A definitive conclusion could not be drawn to asses if the 0.5-cm imagery allows for higher location accuracy, because it performed better in the X compared to the two-cm GCP method, but slightly worse in Y and almost the same in Y as the two-cm RTK method. The two-cm RTK method produced four times more RMSE in the Y component than the same resolution georeferenced with the GCPs, but less than two times the error in X.

The RMSE found in the two-cm RTK imagery (<0.1 m) could be an acceptable georeferencing accuracy for the physiological breeding program at CIMMYT given the efficiency of data capture workflow. In the measurement of accuracy per GCP, considerable differences in the X and Y component were observed, as well as accuracy differences between GCPs. Such accuracy differences rise the question of possible measurement errors, and further future investigation in the accuracy assessment of the RTK workflow is very recommended to substantiate the current results.

For the comparison involving the effect of the different resolution of the imagery, better estimations of height in March eighth were observed in the two-cm GCP model compared to the 0.5-cm GCP, and a remarkable worse estimation was found for 0.5-cm GCP at maturity, but very low number of samples were available. For biomass, low correlation was seen in the estimation for both resolutions with an $R < 0.4$.

Comparing the accuracy of the georeferencing of an image using the same points used as GCPs is not the most objective approach. Only the RTK method is not using these redundant measurements. The use of independent checkpoints should be used for future comparisons.

4.2.4 GLOBAL RESULTS

The objectives of this study were achieved at some extent. The plant height and plot volume estimations were performed using the 3D digital model of the wheat experimental plots at two different resolutions and with two different georeferencing methods using the proposed methods. Comparison between estimated plant height versus the field measurements of plant height resulted in correlations that ranged from moderate to high.

For the comparison between estimated plot volume and field measured biomass, correlations ranged from low to moderately low. The most suitable georeferencing method was found to be the direct RTK geotagging. The most suitable spatial resolution was the two-centimeter imagery for the plant height estimations, but for volume it was not clearly identified, and further research is suggested.

In response to the research questions, it was not yet found that plant height can be estimated with a high enough correlation with this photogrammetric approach to confidently replace manual measurement in wheat physiology experimental plots; it can be estimated moderately well around the stages of anthesis to maturity, but more robust validation is needed before replacing the current workflow.

It was not seen clearly that plant biomass can be estimated accurately enough with this photogrammetric approach to already replace manual measurement in wheat physiology experimental plots, as moderate to low correlations were found. Promising results were obtained, but the number of comparison samples was low in this study and more research is needed clarify this question.

Regarding plant height estimations, the best resolution for the 3D model reconstruction between the two options evaluated is the two centimeter per pixel imagery. However, it is convenient to make more evaluations with more dataset of consistent sample sizes to confirm this result. In relationship to the biomass estimations, no clear best choice was observed, and further research can help clear this question.

The fixed wing UAV used for the two-centimeter imagery acquisition can generate the desired high overlap, however, the UAV had to pass over the area of interest several times to acquire it. This increases the acquisition time and overrides the advantage of the fixed-wing UAV versus the multirotor UAV of fast image acquisition. The fixed-wing UAV can be more useful in fast image acquisition in big areas at moderately high resolutions.

Finally, the RTK correction for the direct georeferencing of the imagery, and thus of the 3D model, was found as accurate as the GCP method for these purposes, being able to replace

it in the data collection workflows for HTP. An optimal use of the RTK correction in the experimental plots for photogrammetry work could be onboard a multiorotor UAV.

Based on the results of the current work, the hypothesis is accepted because there are results that suggest that it is possible to estimate accurately wheat biomass in experimental trials by using the plant height and plot volume through 3D reconstruction made from high resolution images acquired and geotagged with a fixed-wing unmanned aerial vehicle with real time kinematic position correction, without the need of ground control points.

5 CONCLUSIONS

This work focused in the estimation of plant height and biomass in wheat experimental plots using photogrammetry based on aerial imagery acquired with UAV. The focus was in the comparison of two different spatial resolutions for the imagery, *i.e.* two and 0.5 centimeters, and two georeferencing methods, *i.e.* using GCP and direct georeferencing based on the geotagging of the imagery with RTK correction on the UAV.

Correlations in estimations of PH compared to ground measurement ranged from 0.52 to 0.87 for all the methods and georeferencing techniques, excluding one unreliable comparison. The best estimation was with the two-cm GCP imagery close to the maturity stage (R = 0.87), taking the aerial and ground measurement on the same day.

The estimation of AGB from volume resulted in correlations from -0.01 to 0.40 for all the methods and georeferencing techniques. The best estimation was achieved at the anthesis stage with the 0.5-cm GCP imagery (R = 0.4). No observable relation was perceived at the booting stage for any of the remote datasets and the measured data.

Regarding the identification of the most suitable resolution and georeferencing method for the imagery to estimate PH and AGB, the two-cm GCP dataset presented in general the higher correlations and lower RMSE. However, the minor differences between methods made it difficult to select an obvious best option.

The results show the feasibility to obtain plant height estimations on wheat using high-resolution aerial imagery in an experimental field and show the possibility to use the plot volume as a mild estimator of plant biomass at certain stages, *i.e.* from anthesis onwards. However, the experiment also displays the need to carefully consider the key factors to obtain accurate and reliable quality data. More research is needed to validate the use of this HTP workflow in the physiological breeding at the CENEB experimental station as unique source of data for height and above ground biomass of the wheat plots. Validation using LIDAR survey methodologies is suggested for future work.

In the future campaigns, the lessons learned from this work can be implemented. Careful planning of the flight plans will assure a uniform methodology and good data for the analysis. The synchronization of field data measurements with UAV imagery at each growth stage is crucial for the research, however, simultaneous measurements in the field with the imagery capture may introduce noise in the 3D model if the field workers appear in the imagery. The UAV RTK correction for direct georeferencing of the 3D model is a very promising technology that can make the data collection efficient and allow for HTP to use genomic modeling to expedite genetic gains and ensure food security.

6 REFERENCES

Aber, J. S., Marzolff, I., & Ries, J. B. (2010). Small-Format Aerial Photography: Principles, Techniques and Geoscience Applications. Elsevier Science. doi:https://doi.org/10.1016/C2009-0-18493-3

Bareth, G., Bendig, J., Tilly, N., hoffmeister, D., Aasen, H., & Andreas, B. (2016). A Comparison of UAV- and TLS-derived Plant Height for Crop Monitoring: Using Polygon Grids for the Analysis of Crop Surface Models (CSMs). *Photogrammetrie Fernerkundung Geoinformation, 2016*(2), 85-94. doi:10.1127/pfg/2016/0289

Benassi, F., Dall'Asta, E., Diotri, F., Forlani, G., Morra di Cella, U., Roncella, R., & Santise, M. (2017). Testing Accuracy and Repeatability of UAV Blocks Oriented with GNSS-Supported Aerial Triangulation. *Remote sensing, 9*(2), 172. doi:10.3390/rs9020172

Bendig, J., Bolten, A., & Bareth, G. (2013). UAV-based Imaging for Multi-Temporal, very high Resolution Crop Surface Models to monitor Crop Growth Variability. *Photogrammetrie - Fernerkundung - Geoinformation, 2013*(6), 551-562.

Bendig, J., Bolten, A., Bennertz, S., Broscheit, J., Eichfuss, S., & Bareth, G. (2014). Estimating Biomass of Barley Using Crop Surface Models (CSMs) Derived from UAV-Based RGB Imaging. *Remote Sensing, 6*, 10395-10412. doi:doi:10.3390/rs61110395

Berry, P. M., Sterling, M., Baker, C., Spink, J., & Sparkes, D. L. (2003). A calibrated model of wheat lodging compared with field measurements. *Agricultural and Forest Meteorology, 119*, 167-180. doi:10.1016/S0168-1923(03)00139-4

Bivand, R., Keitt, T., & Rowlingson, B. (2018). rgdal: Bindings for the 'Geospatial' Data Abstraction Library. *1.2-18*. Retrieved 06 23, 2019, from https://CRAN.R-project.org/package=rgdal

Brocks, S., & Bareth, G. (2018). Estimating Barley Biomass with Crop Surface Models from Oblique RGB Imagery. *Remote Sensing, 10*(268). doi:10.3390/rs10020268

Brocks, S., Bendig, J., & Bareth, G. (2016). Toward an automated low-cost threedimensional crop surface monitoring system using oblique stereo imagery from consumer-grade smart cameras. *Journal of Applied Remote Sensing, 10*(4), 460214. doi:10.1117/1.JRS.10.046021

Bu, H., Sharma, L. K., Denton, A., & Franzen, D. (2017). Comparison of Satellite Imagery and Ground-Based Active Optical Sensors as Yield Predictors in Sugar Beet, Spring Wheat, Corn, and Sunflower. *Agronomy Journal, 109*, 299–308. doi:10.2134/agronj2016.03.0150

Chapman, S. C., Merz, T., Chan, A., Jackway, P., Hrabar, S., Dreccer, M. F., . . . Jimenez-Berni, J. (2014). Pheno-Copter: A Low-Altitude, Autonomous Remote-Sensing Robotic Helicopter for High-Throughput Field-Based Phenotyping. *Agronomy, 4*, 279-301. doi:10.3390/agronomy4020279

Cheng, L., Jianya, G., Li, M., & Liu, Y. (2011). 3D Building Model Reconstruction from Multi-view Aerial Imagery and Lidar Data. *Photogrammetric Engineering & Remote Sensing, 77*(2), 125-139.

Crain, J. L., Wei, Y., Barker, J., Thompson, S. M., Alderman, P. D., Reynolds, M., . . . Poland, J. (2016). Development and Deployment of a Portable Field Phenotyping Platform. *Crop Science, 56*, :965–975. doi:10.2135/cropsci2015.05.0290

Curtis, B. C., Rajaram, S., & Gómez Macpherson, H. (2002). *Bread Wheat, Improvement and production.* Rome: Food and Agriculture Organization of the United Nations.

Dall'Asta, E., Forlani, G., Roncella, R., Santise, M., Diotri, F., & Morra di Cellab, U. (2017). Unmanned Aerial Systems and DSM matching for rock glacier monitoring. *ISPRS Journal of Photogrammetry and Remote Sensing, 127*, 102-114. doi:10.1016/j.isprsjprs.2016.10.003

De Castro, A. I., Jiménez-Brenes, F. M., Torres-Sánchez, J., Peña, J. M., Borra-Serrano, I., & López-Granados, F. (2018). 3-D Characterization of Vineyards Using a Novel UAV Imagery-Based OBIA Procedure for Precision Viticulture Applications. *Remote Sensing, 10*(4), 584. doi:http://dx.doi.org/10.3390/rs10040584

De Souza, C. H., Camargo Lamparelli, R. A., Rocha, J. V., & Magalhães, P. S. (2017). Height estimation of sugarcane using an unmanned aerial system (UAS) based on structure from motion (SfM) point clouds. *International Journal of Remote Sensing*, 2218-2230.

Deery, D., Jimenez-Berni , J., Jones , H., Sirault, X., & Furbank, R. (2014). Proximal Remote Sensing Buggies and Potential Applications for Field-Based Phenotyping. *Agronomy, 4*(3), 349-379. doi:doi.org/10.3390/agronomy4030349

Devi, S. (2014). Stereoscopic Vision, Stereoscope, Selection of Stereo Pair and Its Orientation. *International Journal of Science and Research, 3*(9), 99-104. Retrieved 06 22, 2019, from https://www.ijsr.net/archive/v3i9/U0VQMTQzOQ==.pdf

FAO, Food and Agriculture Organization of the United Nations. (2017). *The state of food and agriculture: Leveraging food systems for inclusive rural transformation.* United Nations, Food and Agriculture Organization, Rome. Retrieved 09 16, 2018, from http://www.fao.org/3/a-i7658e.pdf

FAO, Food and Agriculture Organization of the United Nations. (2018). *Food Outlook: Biannual Report on Global Food Markets .* United Nations, Food and Agriculture

Organization. Retrieved September 15, 2018, from http://www.fao.org/3/CA0239EN/ca0239en.pdf

FAO - Food and Agriculture Organization of the United Nations, IFAD - International Fund for Agricultural Development, UNICEF - United Nations Children's Fund, WFP - World Food Programme and WHO - World Health Organization. (2018). *The state of food security and nutrition in the world 2018.* Rome: FAO.

Frasco, M. (2018). Metrics: Evaluation Metrics for Machine Learning. *V. 0.1.4*. Retrieved October 11, 2018, from https://www.rdocumentation.org/packages/Metrics/versions/0.1.4

Geipel, J., Link, J., & Claupein, W. (2014). Combined Spectral and Spatial Modeling of Corn Yield Based on Aerial Images and Crop Surface Models Acquired with an Unmanned Aircraft System. *Remote sensing*, 10335-10355. doi:10.3390/rs61110335

Guan, H., Liu, M., Ma, X., & Yu, S. (2018). Three-Dimensional Reconstruction of Soybean Canopies Using Multisource Imaging for Phenotyping Analysis. *Remote Sensing, 10*(8). doi:10.3390/rs10081206

Harwin, S., & Lucieer, A. (2012). Assessing the Accuracy of Georeferenced Point Clouds Produced via Multi-View Stereopsis from Unmanned Aerial Vehicle (UAV) Imagery. *Remote Sensing, 4*(6), 1573-1599.

Heffner, E. L., Sorrells, M. E., & Jannink, J.-L. (2009). Genomic Selection for Crop Improvement. *Crop Science, 49*(1), 1-12. doi:10.2135/cropsci2008.08.0512

Hijmans, R. (2017). Raster: Geographic Data Analysis and Modeling. *R Package*. Retrieved October 12, 2018, from https://CRAN.R-project.org/package=raster

Holman, F. H., Riche , A. B., Michalski, A., Castle, M., Wooster, M. J., & Hawkesford, M. J. (2016). High Throughput Field Phenotyping of Wheat Plant Height and Growth Rate in Field Plot Trials Using UAV Based Remote Sensing. *Remote sensing, 8*(12), 1031. doi:doi:10.3390/rs8121031

Humboldt State University. (n.d.). Vegetation Spectral Reflectance Curves. Introduction to remote sensing: Learning Module 2.1 Interaction of EMR with Earth's Atmosphere and Surfaces. Retrieved June 22, 2019, from: http://gsp.humboldt.edu/OLM/Courses/GSP_216_Online/lesson2-1/vegetation.html

Hurcom, S. J., Harrison, A. R., & Taberner, M. (1996). Assessment of biophysical vegetation properties through spectral decomposition techniques. *Remote Sensing of Environment, 56*, 203–214.

Kemanian, A. R., Stöckle, C. O., Huggins, D. R., & Viega, L. M. (2007). A simple method to estimate harvest index in grain crops. *Field Crops Research, 103*(3), 208-216. doi:doi.org/10.1016/j.fcr.2007.06.007

Lobell, D., Asner, G., Ortiz-Monasterio, J., & Benning, T. (2003). Remote sensing of regional crop production in the Yaqui Valley, Mexico: estimates and uncertainties. *Agriculture, Ecosystems & Environment, 94*(2), 205-220. doi:10.1016/S0167-8809(02)00021-X

Lowe, D. (2004). Distinctive image features from scale-invariant keypoints. *International Journal Computer Vision, 60*, 91–110.

Madec, S., Baret, F., Solan, B., Thomas, S., Dutartre, D., Jezequel, S., . . . Comar, A. (2017). High-Throughput Phenotyping of Plant Height: Comparing Unmanned Aerial Vehicles and Ground LiDAR Estimates. *Frontiers in plant science, 8*(2002). doi:10.3389/fpls.2017.02002

Marshall, D. M., Barnhart, R. K., Hottman, S. B., Shappee, E., & Most, M. T. (Eds.). (2012). *Introduction to unmanned aircraft systems.* Boca Raton: CRC Press.

Matson, P., Luers, A. L., Seto, K. C., Naylor, R. L., & Ortiz-Monasterio, I. J. (2005). People, Land Use, and Environment in the Yaqui Valley, Sonora, Mexico. In B. Entwisle, & P. C. Stern, *Population, Land Use, and Environment: Research Directions* (pp. 238-265). Washington D.C., U.S.A: The National Academies Press.

Mike1024. (2008). LIDAR scanned SICK LMS animation [animated graphic]. *Wikipedia.* Retrieved March 18, 2019, from: https://en.wikipedia.org/wiki/Lidar#/media/File:LIDAR-scanned-SICK-LMS-animation.gif

Monserrat, O., & Crosetto, M. (2008). Deformation measurement using terrestrial laser scanning data and least squares 3D surface matching. *ISPRS Journal of Photogrammetry and Remote Sensing, 63*(1), 142-154. doi:10.1016/j.isprsjprs.2007.07.008

Moore, G. (1979). What is a picture worth? A history of remote sensing / Quelle est la valeur d'une image? Un tour d'horizon de télédétection. *Hydrological Sciences Bulletin, 24*(4), 477-485. doi:10.1080/02626667909491887

NASA, National Aeronautics and Space Administration. (n.d.). Landsat 1. *NASA*: Landsat science. Retrieved July 19, 2019, from https://landsat.gsfc.nasa.gov/landsat-1/

NOAA, National Oceanic and Atmospheric Administration. (n.d.). Differential GPS. Earth Observation in the frame of EO-MINERS - Overview of remote sensing methods, sensors and applications. Retrieved June 22, 2019, from: http://www.eo-miners.eu/earth_observation/eo_eof_msa_forthcoming_review.htm

Pask, A., Joshi, A., Manès, Y., Sharma, Sharma, I., Chatrath, R., . . . Reynolds, M. (2014). A wheat phenotyping network to incorporate physiological traits for climate change in South Asia. *Field Crops Research*, 156-167. doi:http://dx.doi.org/10.1016/j.fcr.2014.07.004

Pask, A., Pietragalla, J., Mullan, D., & Reynolds, M. (Eds.). (2012). *Physiological breeding II: A field guide to wheat phenotyping.* Mexico D.F.: CIMMYT.

Peterson, B., & Carl, P. (2013). PerformanceAnalytics: Econometric Tools for Performance and Risk Analysis. *V 1.1.0*. Retrieved October 10, 2018, from https://CRAN.R-project.org/package=PerformanceAnalytics

Pittman, J. J., Arnall, D. B., Interrante, S. M., Moffet, C. A., & Butler, T. J. (2015). Estimation of Biomass and Canopy Height in Bermudagrass, Alfalfa, and Wheat Using Ultrasonic, Laser, and Spectral Sensors. *Sensors, 15*(2), 2920-2943.

Poynton, C. (2006, 11 28). Color FAQ - Frequently Asked Questions Color. *Poynton*. Retrieved 07 10, 2019, from: http://www.poynton.com/ColorFAQ.html

R Core Team & contributors worldwide. (2017). The R Graphics Devices and Support for Colours and Fonts. grDevices v.*3.4.0*. Retrieved October 11, 2018, from: https://www.rdocumentation.org/packages/grDevices/versions/3.4.0

Reynolds, M., & Langridge, P. (2016). Physiological breeding. *Current Opinion in Plant Biology*, 162–171. doi:10.1016/j.pbi.2016.04.005

Reynolds, M., Pask, A., & Muller, D. (Eds.). (2012). *Physiological Breeding I: Interdisciplinary Approaches to Improve Crop Adaptation.* D.F., Mexico: CIMMYT.

Ruffner, K. C. (Ed.). (1995). *CORONA: America's First Satellite Program.* Washington D.C.: Central Intelligence Agency.

Rutkoski, J., Poland, J., Mondal, S., Autrique, E., González Pérez, L., Crossa, J., . . . Singh, R. (2016). Canopy Temperature and Vegetation Indices from High-Throughput Phenotyping Improve Accuracy of Pedigree and Genomic Selection for Grain Yield in Wheat. *G3: GENES, GENOMES, GENETICS, 6*(9), 2799-2808. doi:10.1534/g3.116.032888

Sanz-Ablanedo, E., Chandler, J., Rodríguez-Pérez, J., & Ordóñez, C. (2018). Accuracy of Unmanned Aerial Vehicle (UAV) and SfM Photogrammetry Survey as a Function of the Number and Location of Ground Control Points Used. *Remote Sensing*, 1606. doi:10.3390/rs10101606

Schirrmann, M., Giebel, A., Gleiniger, F., Pflanz, M., Lentschke, J., & Dammer, K.-H. (2016). Monitoring Agronomic Parameters of Winter Wheat Crops with Low-Cost UAV Imagery. *Remote Sensing, 8*(9).

Science Education through Earth Observation for High Schools. (n.d.). The electromagnetic spectrum and atmospheric transmittance. Introduction to Remote Sensing: 1. Physical Basics, *SEOS Project*. Retrieved June 20, 2019, from: https://seos-project.eu/remotesensing/remotesensing-c01-p01.html

SharkD. (2010a). HSV_color_solid_cylinder [Picture]. Wikimedia commons. Retrieved June 10, 2019, from https://commons.wikimedia.org/w/index.php?curid=9801673, CC BY-SA 3.0

SharkD. (2010b). RGB_color_model [Picture]. Wikimedia commons. Retrieved June 10, 2019, from https://commons.wikimedia.org/w/index.php?curid=3375025, CC BY-SA 4.0

Shi, Y., Thomasson, J. A., Murray, S. C., Pugh, N. A., Rooney, W. L., Shafian, S., . . . Bagavathiannan, M. V. (2016). Unmanned Aerial Vehicles for High-Throughput Phenotyping and Agronomic research. *PLOS ONE*. doi:0.1371/journal.pone.0159781

TheHighTechHobbyist. (2016). Drone Photogrammetry: Make 3D Landscapes. *thehightechhobbyist.* Retrieved June 22, 2019, from: http://thehightechhobbyist.com/drone-photogrammetry/

Tilly, N., Schiedung, H., Hoffmeister, D., & Hütt, C. (2014). Terrestrial laser scanning for plant height measurement and biomass. *The International Archives of the Photogrammetry, Remote Sensing and Spatial Information Sciences.* Istanbul. doi:10.5194/isprsarchives-XL-7-181-2014

Tzounis, A., Katsoulas, N., Bartzanas, T., & Kittas, C. (2017). Internet of Things in agriculture, recent advances and future challenges. *Biosystems Engineering*, 31-48. doi:10.1016/j.biosystemseng.2017.09.007

UN, United Nations. (2015). *Transforming our world: the 2030 agenda for sustainable development A/RES/70/1.* United Nations. Retrieved 06 18, 2019, from https://undocs.org/A/RES/70/1

Walter, J., Edward, J., McDonald, G., & Kuchel, H. (2018). Photogrammetry for the estimation of wheat biomass and harvest index. *Field Crops Research, 216*, 165–174. doi:10.1016/j.fcr.2017.11.024

Wenzhu, Y., Wang, S., Zhao, X., Zhang, J., & Feng, J. (2015). Greenness identification based on HSV decision tree. *Information Processing in Agriculture, 2*(3-4), 149-160. doi:https://doi.org/10.1016/j.inpa.2015.07.003

7 APPENDIX

APPENDIX A – FLIGHT AND WHEATHER CONDITIONS FOR THE FIXED WING DRONE CAMPAIGN

Table 11. Table of the conditions for the flights performed with the fixed wing drone.

Day	Hour	Flight time (min)	Number of images	Average flight height (m)	Sky conditions	Wind speed (m/s)	Origin direction of wind	GSD (cm)
25/01/2017	10:40	17	55	52	Cloudy	4	NW	2
23/01/2017	-	-	115	-	-	-	-	2
27/01/2017	11:50	35.5*	100	60	Clear	7	NW	2
10/02/2017	10:42	26.5*	66	65	Cirrus	4	SE	2
13/02/2017	-	-	42	65	Clear	3	W	2
15/02/2017	12:15	34*	87	65	Clouds	3	SW	2
20/02/2017	-	-	121	-	Clear	4	W	2
22/02/2017	10:21	16	75	65	Clear	2	SW	2
08/03/2017	11:28	36*	170	65	Clouds	1.5	W	2
30/03/2017	12:03	13.5	172	65	-	-	W	2

* Data acquisition performed in two flights. – Data not available.

APPENDIX B – RESIDUALS OF THE DIFFERENCE IN LOCATION BETWEEN GEOREFERENCING METHODS

Table 12. Results of the GCP residuals of the two-cm GCP image from February 13.

X Image	Y Image	X GCP	Y GCP	residual x	residual y
605,948.74	3,030,681.75	605,948.75	3,030,681.73	-0.009	0.018
606,037.08	3,030,682.77	606,037.10	3,030,682.79	-0.023	-0.018
606,035.67	3,030,756.09	606,035.65	3,030,756.06	0.021	0.026
605,947.19	3,030,754.64	605,947.20	3,030,754.62	-0.013	0.022
605,991.42	3,030,755.17	605,991.46	3,030,755.17	-0.041	0.004
605,993.09	3,030,682.32	605,993.10	3,030,682.33	-0.013	-0.007
605,992.31	3,030,716.44	605,992.31	3,030,716.42	0.004	0.017

85

Table 13. Results of the GCP residuals of the two-cm RTK image from February 13.

X Image	Y Image	X GCP	Y GCP	residual x	residual y
605,948.74	3,030,681.75	605,948.75	3,030,681.73	-0.062	0.047
606,037.08	3,030,682.77	606,037.10	3,030,682.79	-0.115	-0.016
606,035.67	3,030,756.09	606,035.65	3,030,756.06	-0.084	0.021
605,947.19	3,030,754.64	605,947.20	3,030,754.62	-0.068	0.021
605,991.42	3,030,755.17	605,991.46	3,030,755.17	-0.111	0.003
605,993.09	3,030,682.32	605,993.10	3,030,682.33	-0.075	0.022
605,992.31	3,030,716.44	605,992.31	3,030,716.42	-0.073	0.012

Table 14. Results of the GCP residuals of the 0.5-cm GCP image from February 13.

X Image	Y Image	X GCP	Y GCP	residual x	residual y
605948.745	3,030,681.75	605,948.75	3,030,681.73	0.008	-0.019
606,037.08	3,030,682.77	606,037.10	3,030,682.79	-0.003	0.022
606,035.67	3,030,756.09	606,035.65	3,030,756.06	-0.022	-0.002
605,947.19	3,030,754.64	605,947.20	3,030,754.62	-0.016	0.017
605,991.42	3,030,755.17	605,991.46	3,030,755.17	-0.002	0.017
605,993.09	3,030,682.32	605,993.10	3,030,682.33	0.010	-0.029
605,992.31	3,030,716.44	605,992.31	3,030,716.42	-0.004	0.045

Table 15. RMSE in X and Y for the two-cm RTK imagery compared to the GCP coordinates

GCP number	RMSE_X	RMSE_Y
1	0.035	0.037
2	0.078	0.010
3	0.040	0.035
4	0.070	0.050
5	0.100	0.025
6	0.060	0.023
7	0.075	0.056
Total	0.065	0.034